IEEE Access
Multidisciplinary ⋮ Rapid Review ⋮ Open Access Journal

Received 5 December 2023, accepted 18 December 2023, date of publication 25 December 2023,
date of current version 12 January 2024.

Digital Object Identifier 10.1109/ACCESS.2023.3347041

METHODS

Hybrid Beamforming Based SWIPT System Satisfying Individual Rate and Energy Constraints

SEONG HWAN KIM[1], (MEMBER, IEEE), AND HU JIN[2,3], (Senior Member, IEEE)
[1]Department of Artificial Intelligence and Data Engineering, Korea National University of Transportation, Uiwang 16106, Republic of Korea
[2]College of Computer and Information Engineering, Henan Normal University, Xinxiang 453007, China
[3]School of Electrical Engineering, Hanyang University, ERICA Campus, Ansan 15588, Republic of Korea

Corresponding author: Hu Jin (hjin@hanyang.ac.kr)

This was supported partially by Korea National University of Transportation Industry-Academy Cooperation Foundation in 2021; in part by the Korea Evaluation Institute of Industrial Technology (KEIT) Grant funded by the Korean Government [(KCG, MOIS, and NFA) RS-2022-001549812 Development of Technology to respond to marine fires and chemical accidents using wearable devices]; and in part by the National Research Foundation of Korea (NRF) Grant funded by the Korean Government through MSIT under Grant NRF-2022R1F1A1071093.

ABSTRACT In this paper, we consider a simultaneous wireless information and power transfer (SWIPT) system adopting hybrid analog-digital beamforming where a base station (BS) with massive antennas transmits different data streams to multiple single-antenna devices. Our primary objective is to minimize the transmit-power of the BS while ensuring energy harvesting and signal-to-interference-plus-noise ratio (SINR) requirements of each device. We specifically highlight that our approach can accommodate the scenarios where users have different requirements on the harvested energy and the received SINR. We propose two suboptimal solutions in which digital and analog precoders are designed jointly. In the first solution (OptDig-ProRF), the objective function is approximated to be independent of the digital precoder and power splitting ratios, and the local minimum of the objective function is found to obtain an analog precoder. Subsequently, the optimal digital precoder and power splitting ratios are found for the obtained analog precoder using semidefinite relaxation of the original problem. In the second solution (ZfDig-SohRF), to reduce computational complexity, we newly design a zero-forcing (ZF) digital precoder which meets users' requirements while applying the corresponding analog precoder proposed in the literature. The two precoders are iteratively found until the transmit power difference between two consecutive updates falls below a threshold. Illustrative results show that the OptDig-ProRF scheme yields a very close performance to the fully digital precoder in terms of transmit power, while the ZfDig-SohRF scheme outperforms the optimal digital precoder plus a conventional analog precoder scheme at high SINR constraints.

INDEX TERMS SWIPT, hybrid beamforming, individual requirements.

I. INTRODUCTION

The Internet of Things (IoT) is revolutionizing various industries. Nevertheless, powering a multitude of IoT devices remains a significant challenge due to its impact on maintenance costs and the longevity of IoT networks. A compelling solution to this obstacle is energy harvesting (EH), which harnesses electromagnetic signals to transmit energy to devices located far from a transmitter, enabling the implementation of battery-free IoT devices [1], [2]. Recently, the International Telecommunication Union Radio Communication Sector (ITU-R) highlighted battery-free devices as a promising technology candidate for 6G in their report [3]. In addition, ambient power-enabled IoT is actively discussed as a study item for 3GPP release 19 known as 5G-Advanced [4]. EH is also attracting substantial attention from academia and industries under various names such as zero-energy devices and batteryless devices [5], [6], [7], [8].

To enable efficient management of massive connectivity by the base station (BS), the BS needs to employ a

The associate editor coordinating the review of this manuscript and approving it for publication was Jun Cheng.

radio frequency (RF) for both information transmission and energy transfer. This concept, known as simultaneous wireless information and power transfer (SWIPT), can be realized through three primary receiver designs: time switching (TS), antenna switching (AS), and power-splitting (PS) [8]. The TS structure allows a receiver to alternate between information decoding (ID) and energy harvesting (EH), necessitating fine time synchronization and a guard time to account for propagation delay. In the AS structure, multiple antennas embedded in an IoT device are split into the EH and ID purposes. However, this multi-antenna configuration comes with costs and finely adjusting the ID and EH levels is challenging. The PS structure entails a power splitter within a receiver to partition the signal for EH and ID objectives. Among these three, the PS-based design is deemed more practical due to its robustness against coarse time synchronization and its flexibility in adjusting the ID-to-EH ratio [9]. As a consequence, we also focus on the PS-based SWIPT (PS-SWIPT) system in this paper.

Since the integration of multiple antennas has been shown to yield significant spectral and energy efficiency gains in wireless communication systems, the initial SWIPT study was considered in multi-input-multiple-output (MIMO) environments [10]. In [11], the PS-SWIPT was applied to downlink multi-user multi-input-single-output (MU-MISO) systems where a BS equipped with multiple antennas supports multiple single-antenna receivers. Their primary objective is to minimize the transmit-power by jointly optimizing the transmit beamforming vectors and power-splitting ratios while guaranteeing signal-to-interference-plus-noise ratio (SINR) and harvested energy requirements of each user. Zong et al. [12] extended the work in [11] into K-user multiple-input-multiple-output (MIMO) interference channels and jointly designed receive filters, transmit beamformers, and power splitters. In [13], the SWIPT system was explored in the context of user-centric BS clustering for dense networks. Furthermore, the SWIPT has been researched in the context of intelligent reflecting surface (IRS)-aided networks [14], non-orthogonal multiple access (NOMA) [15], and coordinated multi-point (CoMP) systems [16].

Indeed, the use of large-scale antenna arrays in conjunction with proper beamforming techniques provides substantial degrees of freedom [17], [18]. However, this advantage comes with increased hardware cost and higher power consumption. To address the cost challenges associated with fully digital beamforming, researchers have explored the concept of an analog-digital hybrid beamforming structure [19], [20], [21], [22], [23], [24], [25], [26], [27]. In this approach, the beamforming process is partitioned into a conventional digital domain and an analog domain that employs phase shifters, which is more economical as the number of RF chains is reduced compared to fully digital beamforming. However, this leads to a trade-off, resulting in performance degradation due to the constraint of unit-magnitude-entry placed on the elements of the analog beamformer. The hybrid beamforming structure has been investigated extensively in downlink multiuser millimeter-wave (mmWave) systems with the aim of maximizing the sum-rate for both single-antenna users [22] and multi-antenna users [23]. Additionally, it has been explored for maximizing the minimum rates among the users [24]. Chen et al. [25] tried to optimally allocate data streams of multiple users to subcarriers for minimizing transmit-power in the context of mmWave communications. It is notable that the hybrid beamforming structure was already adopted by the current 5G New Radio (NR) systems.

There has been numerous studies on downlink SWIPT systems with the hybrid beamforming structure [28], [29], [30], [31]. In [28], the authors proposed a hybrid beamforming design aimed at minimizing transmit power in an MU-MISO SWIPT system. They impose a limitation on users' capabilities, allowing each user to either receive information or harvest energy, but not both simultaneously. In [29], the authors considered hybrid beamforming for the PS-SWIPT system in the context of multi-group multicast communications. Their approach incorporates limitations on antenna configurations for the sake of simplicity. Specifically, the output of each RF chain is connected to only a portion of the transmit antennas, rather than all of them. In contrast, our approach considers a fully connected hybrid beamforming structure, enhancing the flexibility and performance of the system. Kwon et al. [30] studied the hybrid beamforming SWIPT system to maximize the weighted sum of achievable rates and harvested power of all users under a total power constraint. However, this approach cannot provide a solution for addressing the distinct rate and energy requirements of individual IoT devices.

In this paper, we investigate the hybrid beamforming MU-MISO PS-SWIPT system, where a BS equipped with massive antennas serves multiple single-antenna IoT devices. Unlike the approach in [28], we assume that each device possesses the capability to receive both information and energy simultaneously, thereby making our design applicable to future battery-free IoT devices. Our primary goal is to minimize the transmit power of the BS. The pursuit of transmit power minimization holds significant importance for two key reasons. Firstly, reducing transmit power contributes to a decrease in intercell interference, thereby enhancing the overall performance of the cellular system. Secondly, this approach yields lower CO_2 emissions, thus aligning with environmentally sustainable strategies. Furthermore, we place a strong emphasis on ensuring individualized constraints on harvested energy and SINR of each user. These individualized constraints are beneficial for accommodating diverse use cases, different specifications, and the dynamic environmental conditions expected in future IoT networks. We propose two suboptimal solutions for designing digital and analog precoders of the hybrid beamforming. In the *first* solution, the objective function is approximated to be irrelevant to the digital precoder and power splitting ratios,

and the local minimum of the objective function is found to obtain an analog precoder. Subsequently, the optimal digital precoder and power splitting ratios are obtained for the acquired analog precoder using semidefinite relaxation of the original problem. We also provide the feasibility condition of the optimal digital precoder design in the first solution. In the *second* solution, to reduce computational complexity, we newly design a zero-forcing (ZF) digital precoder that meets users' requirements and apply the corresponding analog precoder to the ZF precoder.[1] The two precoders are iteratively found until the transmit power difference between two consecutive updates falls below a threshold.

The rest of this paper is organized as follows. In Section II, we describe the system model of an analog-digital hybrid precoding in downlink MU-MISO systems and formulate a transmit-power minimization problem. In Section III, the solution with the optimal digital precoder is proposed. In Section IV, the solution with the ZF digital precoder is proposed. We present illustrative results in Section VI. Finally, we present concluding remarks in Section VII.

Throughout this paper, we use the following notation. Normal letters represent scalar quantities, boldface lowercase letters indicate vectors and boldface uppercase letters designate matrices. The trace, transpose, and Hermitian transpose are represented by $\mathrm{Tr}(\cdot)$, $(\cdot)^T$, and $(\cdot)^H$, respectively. The expectation operation and the Euclidean 2-norm of a vector are denoted by $\mathbb{E}[\cdot]$ and $\|\cdot\|$, respectively. $\mathbf{I}_n$ denotes an identity matrix of size n. We use $\mathbf{z} \sim \mathcal{CN}(\mathbf{0}, \Sigma)$ to denote a circularly symmetric complex Gaussian vector $\mathbf{z}$ with zero mean and covariance matrix Σ. $\boldsymbol{A}_k$ denotes the k-th column of matrix $\boldsymbol{A}$. $\boldsymbol{A}(i,j)$ is the element at the ith row and the jth column. $\boldsymbol{A} \succeq \mathbf{0}$ denotes that $\boldsymbol{A}$ is a positive semidefinite matrix.

II. SYSTEM MODEL

We consider a downlink MU-MISO system with K single-antenna users where a hybrid precoding technique is introduced at the BS. The received signal at each single-antenna user is split into two parts, one is for ID and another one is for EH. The BS has N transmit antennas and N_{RF} RF chains where $N \geq N_{\mathrm{RF}}$.

A. SIGNAL MODEL

The BS uses a digital precoder, $\boldsymbol{V}_{\mathrm{Dig}} \in \mathbb{C}^{N_{\mathrm{RF}} \times K}$, and an analog precoder, $\boldsymbol{V}_{\mathrm{RF}} \in \mathbb{C}^{N \times N_{\mathrm{RF}}}$ with $|\boldsymbol{V}_{\mathrm{RF}}(i,j)|^2 = 1, \forall i,j$. A transmitted signal is written as

$$\boldsymbol{x} = \boldsymbol{V}_{\mathrm{RF}} \boldsymbol{V}_{\mathrm{Dig}} \boldsymbol{s}, \tag{1}$$

where $\boldsymbol{s} = [s_1 \ s_2 \ \cdots \ s_K]^T$ and s_k denotes the data symbol for user k. We assume $\mathbb{E}[\boldsymbol{s}\boldsymbol{s}^H] = \mathbf{I}_K$. The received signal at user k is expressed as

$$y_k = \boldsymbol{h}_k^H \boldsymbol{x} + n_{A,k}, \tag{2}$$

[1]This analog precoder was previously proposed in the literature [22].

where $\boldsymbol{h}_k^H \in \mathbb{C}^{1 \times N}$ denotes the channel vector for user k and $n_{A,k} \sim \mathcal{CN}(0, \sigma_k^2)$ denotes the antenna noise at user k. The power slitting ratio of user k is denoted by ρ_k, meaning that ρ_k portion of the signal power is allocated to the ID and $1-\rho_k$ portion to the EH. Then, the two received signals for the ID and ED processes are given by

$$\begin{aligned} y_k^{\mathrm{ID}} &= \sqrt{\rho_k}(\boldsymbol{h}_k^H \boldsymbol{V}_{\mathrm{RF}} \boldsymbol{V}_{\mathrm{Dig}} \boldsymbol{s} + n_{A,k}) + n_{S,k} \\ &= \underbrace{\sqrt{\rho_k} \boldsymbol{h}_k^H \boldsymbol{V}_{\mathrm{RF}} \boldsymbol{V}_{\mathrm{Dig},k} s_k}_{\text{desired signal}} \\ &\quad + \underbrace{\sqrt{\rho_k} \sum_{l \neq k}^{K} \boldsymbol{h}_k^H \boldsymbol{V}_{\mathrm{RF}} \boldsymbol{V}_{\mathrm{Dig},l} s_l}_{\text{interference}} + \sqrt{\rho_k} n_{A,k} + n_{S,k}, \end{aligned} \tag{3}$$

$$y_k^{\mathrm{EH}} = \sqrt{1-\rho_k}(\boldsymbol{h}_m^H \boldsymbol{V}_{\mathrm{RF}} \boldsymbol{V}_{\mathrm{Dig}} \boldsymbol{s} + n_{A,k}), \tag{4}$$

respectively, where $n_{S,k} \sim \mathcal{CN}(0, \delta_k^2)$ denotes the additional noise introduced by the ID process at user k and $\boldsymbol{V}_{\mathrm{Dig},k}$ denotes the kth column of $\boldsymbol{V}_{\mathrm{Dig}}$. The SINR of user k is expressed by

$$SINR_k = \frac{\rho_k \|\boldsymbol{h}_k^H \boldsymbol{V}_{\mathrm{RF}} \boldsymbol{V}_{\mathrm{Dig},k}\|^2}{\rho_k \sum_{l \neq k}^{K} \|\boldsymbol{h}_k^H \boldsymbol{V}_{\mathrm{RF}} \boldsymbol{V}_{\mathrm{Dig},l}\|^2 + \rho_k \sigma_k^2 + \delta_k^2}. \tag{5}$$

The harvested energy at user k is given by

$$E_k = \eta_k (1-\rho_k) \left(\sum_{l=1}^{K} \|\boldsymbol{h}_k^H \boldsymbol{V}_{\mathrm{RF}} \boldsymbol{V}_{\mathrm{Dig},l}\|^2 + \sigma_k^2 \right), \tag{6}$$

where η_k denotes the energy transfer efficiency of user k.

B. PROBLEM FORMULATION

We are interested in minimizing the transmit power of the BS, $\mathrm{Tr}(\boldsymbol{V}_{\mathrm{RF}} \boldsymbol{V}_{\mathrm{Dig}} \boldsymbol{V}_{\mathrm{Dig}}^H \boldsymbol{V}_{\mathrm{RF}}^H)$, while guaranteeing the SINR and harvested energy requirements of each user when the instantaneous channel matrix $\boldsymbol{H} = [\boldsymbol{h}_1, \cdots, \boldsymbol{h}_K]^H$ is known to the BS. That is, we aim to find the optimal analog precoder, digital precoder, and power splitting ratios by solving the following problem:

$$\min_{\{\boldsymbol{V}_{\mathrm{RF}}, \boldsymbol{V}_{\mathrm{Dig}}, \rho_k\}} \quad \mathrm{Tr}(\boldsymbol{V}_{\mathrm{RF}} \boldsymbol{V}_{\mathrm{Dig}} \boldsymbol{V}_{\mathrm{Dig}}^H \boldsymbol{V}_{\mathrm{RF}}^H) \tag{7a}$$

$$\text{s. t.} \quad \mathrm{SINR}_k \geq \gamma_k, \quad \forall k, \tag{7b}$$

$$\mathrm{E}_k \geq e_k, \quad \forall k, \tag{7c}$$

$$|\boldsymbol{V}_{\mathrm{RF}}(i,j)|^2 = 1, \quad \forall i,j, \tag{7d}$$

$$0 < \rho_k < 1. \quad \forall k. \tag{7e}$$

The problem (7) is non-convex and has variables $\boldsymbol{V}_{\mathrm{RF}}$, $\boldsymbol{V}_{\mathrm{Dig}}$, and $\{\rho_k\}$ coupled to each other, so that the problem is intractable. We propose two suboptimal solutions in the following Sections III and IV.

C. A REFERENCE FULLY DIGITAL PRECODER

A fully digital precoder, where the number of RF chains is the same as that of antennas, always outperforms a hybrid

precoder which has a smaller number of RF chains than that of antennas. Therefore, the performance of a SWIPT system with a fully digital precoder shows an upper-bound to the performance of a hybrid precoder. Let us denote $\boldsymbol{V}_{\text{Full}} \in \mathbb{C}^{N\times K}$ as a fully digital precoding matrix, then a power minimization problem with it can be formulated as

$$\min_{\{\boldsymbol{V}_{\text{Full}}\}} \quad \text{Tr}(\boldsymbol{V}_{\text{Full}}\boldsymbol{V}_{\text{Full}}^H) \tag{8a}$$

$$\text{s. t.} \quad \frac{\rho_k \|\boldsymbol{h}_k^H \boldsymbol{V}_{\text{Full},k}\|^2}{\rho_k \sum_{l\neq k}^{K} \|\boldsymbol{h}_k^H \boldsymbol{V}_{\text{Full},l}\|^2 + \rho_k\sigma_k^2 + \delta_k^2} \geq \gamma_k, \quad \forall k, \tag{8b}$$

$$\eta_k(1-\rho_k)\left(\sum_{l=1}^{K} \|\boldsymbol{h}_k^H \boldsymbol{V}_{\text{Full},l}\|^2 + \sigma_k^2\right) \geq e_k, \quad \forall k, \tag{8c}$$

$$0 < \rho_k < 1. \quad \forall k. \tag{8d}$$

The optimal solution of problem (8) has been found using the technique of semidefinte relaxation (SDR) in [11].

III. HYBRID BEAMFORMING SWIPT WITH OPTIMAL DIGITAL PRECODER

In this section, for the problem (7), we propose one sub-optimal solution in which the digital and analog precoders are separately found. At first, we develop a methodology of finding an analog precoder $\boldsymbol{V}_{\text{RF}}$ that is independent from the digital precoder. While this analog precoder is suboptimal, its implementation complexity can be reduced significantly due to the independence and the performance degradation is minimal which will be shown in Section V. Then, based on the analog precoder obtained, we find the corresponding optimal digital precorder $\boldsymbol{V}_{\text{Dig}}$ and power splitting ratios $\{\rho_k\}$.

A. ANALOG PRECODER DESIGN

We begin by assuming that $\boldsymbol{V}_{\text{Dig}}$ and $\{\rho_k\}$ are given and postpone the discussion of finding their optimal values to the next subsection. Letting $\boldsymbol{X}_k \triangleq \boldsymbol{V}_{\text{Dig},k}\boldsymbol{V}_{\text{Dig},k}^H$ for all k, problem (7) is reformulated as

$$\min_{\boldsymbol{V}_{\text{RF}}} \quad \text{Tr}(\boldsymbol{V}_{\text{RF}} \sum_{k=1}^{K} \boldsymbol{X}_k \boldsymbol{V}_{\text{RF}}^H) \tag{9a}$$

$$\text{s.t.} \quad \frac{\rho_k \boldsymbol{h}_k^H \boldsymbol{V}_{\text{RF}} \boldsymbol{X}_k \boldsymbol{V}_{\text{RF}}^H \boldsymbol{h}_k}{\rho_k \sum_{l\neq k}^{K} \boldsymbol{h}_k^H \boldsymbol{V}_{\text{RF}} \boldsymbol{X}_l \boldsymbol{V}_{\text{RF}}^H \boldsymbol{h}_k + \rho_k\sigma_k^2 + \delta_k^2} \geq \gamma_k, \quad \forall k, \tag{9b}$$

$$\eta_k(1-\rho_k)\left(\sum_{l=1}^{K} \boldsymbol{h}_k^H \boldsymbol{V}_{\text{RF}} \boldsymbol{X}_l \boldsymbol{V}_{\text{RF}}^H \boldsymbol{h}_k + \sigma_k^2\right) \geq e_k, \forall k, \tag{9c}$$

$$|\boldsymbol{V}_{\text{RF}}(i,j)|^2 = 1, \quad \forall i,j. \tag{9d}$$

Assuming the phase of each element in $\boldsymbol{V}_{\text{RF}}$ is i.i.d., we obtain $\boldsymbol{V}_{\text{RF}}^H\boldsymbol{V}_{\text{RF}} \to N\boldsymbol{I}_{N_{\text{RF}}}$ by the law of large number as N goes to infinity. Similarly, we also obtain $\boldsymbol{V}_{\text{RF}}\boldsymbol{V}_{\text{RF}}^H \to N_{\text{RF}}\boldsymbol{I}_N$ as $N_{\text{RF}} \to \infty$. In addition, assuming elements of $\boldsymbol{X}_1, \cdots, \boldsymbol{X}_K$ at the ith row and jth column are i.i.d. complex random variables with zero-mean for $i \neq j$ and with a mean value of β for $i = j$, we obtain $\frac{1}{K}\sum_{k=1}^{K} \boldsymbol{X}_k \to \beta\boldsymbol{I}_{N_{\text{RF}}}$ as $K \to \infty$, where $\beta = \frac{1}{KN_{\text{RF}}}\sum_{k=1}^{K}\sum_{i=1}^{N_{\text{RF}}} \boldsymbol{X}_k(i,i)$. Note that the inequality condition, $0 < \frac{K}{N} \leq \frac{N_{\text{RF}}}{N} < 1$ is still maintained as $K, N_{\text{RF}}, N \to \infty$. Under these assumptions, problem (9) can be rewritten as

$$\min_{\{\boldsymbol{V}_{\text{RF}}\}} \quad \text{Tr}(NK\beta\boldsymbol{I}_{N_{\text{RF}}}) \tag{10a}$$

$$\text{s.t.} \quad (1+\gamma_k)\boldsymbol{h}_k^H \boldsymbol{V}_{\text{RF}} \boldsymbol{X}_k \boldsymbol{V}_{\text{RF}}^H \boldsymbol{h}_k \geq \gamma_k\left(\frac{\delta_k^2}{\rho_k} + \sigma_k^2\right) + \gamma_k KN_{\text{RF}}\beta\boldsymbol{h}_k^H\boldsymbol{h}_k, \forall k, \tag{10b}$$

$$KN_{\text{RF}}\beta\boldsymbol{h}_k^H\boldsymbol{h}_k \geq \frac{e_k}{\eta_k(1-\rho_k)} - \sigma_k^2, \quad \forall k \tag{10c}$$

$$|\boldsymbol{V}_{\text{RF}}(i,j)|^2 = 1, \quad \forall i,j. \tag{10d}$$

We can see that the objective function and constraint (10c) are not related with $\boldsymbol{V}_{\text{RF}}$ while (10b) is. Then, problem (10) becomes a feasibility problem with the SINR constraints as follows

$$\text{find} \quad \boldsymbol{V}_{\text{RF}} \tag{11a}$$

$$\text{s.t.} \quad f_k(\boldsymbol{V}_{\text{RF}}) \geq d_k, \quad \forall k, \tag{11b}$$

$$|\boldsymbol{V}_{\text{RF}}(i,j)|^2 = 1, \quad \forall i,j, \tag{11c}$$

where

$$f_k(\boldsymbol{V}_{\text{RF}}) = \boldsymbol{h}_k^H \boldsymbol{V}_{\text{RF}} \boldsymbol{X}_k \boldsymbol{V}_{\text{RF}}^H \boldsymbol{h}_k$$

$$d_k = \frac{\gamma_k}{(1+\gamma_k)}\left\{\left(\frac{\delta_k^2}{\rho_k} + \sigma_k^2\right) + KN_{\text{RF}}\beta\boldsymbol{h}_k^H\boldsymbol{h}_k\right\}.$$

As $\gamma_k \to \infty$, $\delta_k \to 0$, and $\sigma_k \to 0$, the problem (11) can be reformulated as

$$\text{find} \quad \boldsymbol{V}_{\text{RF}} \tag{12a}$$

$$\text{s.t.} \quad \boldsymbol{h}_k^H \boldsymbol{V}_{\text{RF}} \boldsymbol{X}_k \boldsymbol{V}_{\text{RF}}^H \boldsymbol{h}_k \geq KN_{\text{RF}}\beta\boldsymbol{h}_k^H\boldsymbol{h}_k, \quad \forall k, \tag{12b}$$

$$|\boldsymbol{V}_{\text{RF}}(i,j)|^2 = 1, \quad \forall i,j. \tag{12c}$$

Now, we need to find $\boldsymbol{V}_{\text{RF}}$ which ensures that the received power of user k is equal to or higher than the asymptotic power of interference to user k. Unfortunately, the asymptotic approximations in inequality constraints from the problem (9) to (12) cannot be directly applied to non-asymptotic cases. Instead, we propose a heuristic approach that transforms a feasibility problem with multiple asymptotic constraints into a maximization problem of a single utility function such as

$$\max_{\boldsymbol{V}_{\text{RF}}} \log\left|\boldsymbol{H}\boldsymbol{V}_{\text{RF}}\boldsymbol{V}_{\text{RF}}^H\boldsymbol{H}^H\right| \tag{13a}$$

$$\text{s.t.} \quad |\boldsymbol{V}_{\text{RF}}(i,j)|^2 = 1, \quad \forall i,j, \tag{13b}$$

where $\boldsymbol{H} = [\boldsymbol{h}_1, \cdots, \boldsymbol{h}_K]^H$ and the digital precoder is disregarded to account for the fact that $\boldsymbol{X}_k$ is not optimized at

the early or middle stages of the search. The utility function of problem (13) can be regarded as the asymptotic capacity of (K, N_{RF}) MIMO channel with a channel matrix $\boldsymbol{H}\boldsymbol{V}_{\mathrm{RF}}$ for high signal-to-noise ratio (SNR) and a unit power allocation. Problem (13) is still non-convex and too complex to adjust all elements of $\boldsymbol{V}_{\mathrm{RF}}$ at the same time. Instead, we adjust only $\boldsymbol{V}_{\mathrm{RF}}(i,j)$ assuming all other elements of $\boldsymbol{V}_{\mathrm{RF}}$ are fixed and repeat it over all i and j one by one. For given i and j, from the results in Appendix A, the problem of adjusting $\boldsymbol{V}_{\mathrm{RF}}(i,j)$ can be expressed as

$$\max_{\boldsymbol{V}_{\mathrm{RF}}(i,j)} \ \mathrm{Re}\left\{\chi_{i,j}\boldsymbol{V}_{\mathrm{RF}}(i,j)\right\} \tag{14}$$

where $\chi_{i,j}$ is defined in Appendix A. The solution of (14) is simply written as

$$\boldsymbol{V}_{\mathrm{RF}}(i,j) = \frac{\chi_{i,j}^*}{|\chi_{i,j}|}. \tag{15}$$

Note that an initial value of $\boldsymbol{V}_{\mathrm{RF}}(i,j)$ is necessary in order to apply the solution in (15). We propose to use one CAZAC sequence as the first row of an initial $\boldsymbol{V}_{\mathrm{RF}}$ and place circularly shifted versions of the sequence at next rows of $\boldsymbol{V}_{\mathrm{RF}}$. This initialization satisfies the constraint of unit-magnitude-entry in $\boldsymbol{V}_{\mathrm{RF}}$. In the following subsection III-B, we find the optimal digital precoder for a given $\boldsymbol{V}_{\mathrm{RF}}$ and also prove that the optimal one can be obtained all the time if $\mathrm{rank}(\boldsymbol{V}_{\mathrm{RF}}) = N_{\mathrm{RF}}$ through Proposition 1. The initialization of $\boldsymbol{V}_{\mathrm{RF}}$ using CAZAC sequence satisfies the condition, $\mathrm{rank}(\boldsymbol{V}_{\mathrm{RF}}) = N_{\mathrm{RF}}$. Note that the initialization of $\boldsymbol{V}_{\mathrm{Dig}}$ is not necessary. Since an update of any element in $\boldsymbol{V}_{\mathrm{RF}}$ using (15) does not make the object function of problem (13) lower, i.e., $\left|\boldsymbol{H}\boldsymbol{V}_{\mathrm{RF}}^{(t)}\boldsymbol{V}_{\mathrm{RF}}^{(t)H}\boldsymbol{H}^H\right| \le \left|\boldsymbol{H}\boldsymbol{V}_{\mathrm{RF}}^{(t+1)}\boldsymbol{V}_{\mathrm{RF}}^{(t+1)H}\boldsymbol{H}^H\right|$ where $\boldsymbol{V}_{\mathrm{RF}}^{(t)}$ is the tth updated version of $\boldsymbol{V}_{\mathrm{RF}}$, we update $\boldsymbol{V}_{\mathrm{RF}}$ until the objective function converges to a certain value.

B. OPTIMAL DIGITAL PRECODER

For a given analog precoder and letting $\boldsymbol{X}_k \triangleq \boldsymbol{V}_{\mathrm{Dig},k}\boldsymbol{V}_{\mathrm{Dig},k}^H$, $\forall k$, problem (7) is written as

$$\min_{\{\boldsymbol{X}_k,\rho_k\}} \ \mathrm{Tr}(\boldsymbol{V}_{\mathrm{RF}}\sum_{k=1}^{K}\boldsymbol{X}_k\boldsymbol{V}_{\mathrm{RF}}^H) \tag{16a}$$

$$\text{s.t.} \quad \frac{\rho_k\boldsymbol{h}_k^H\boldsymbol{V}_{\mathrm{RF}}\boldsymbol{X}_k\boldsymbol{V}_{\mathrm{RF}}^H\boldsymbol{h}_k}{\rho_k\sum_{l\neq k}^{K}\boldsymbol{h}_k^H\boldsymbol{V}_{\mathrm{RF}}\boldsymbol{X}_l\boldsymbol{V}_{\mathrm{RF}}^H\boldsymbol{h}_k + \rho_k\sigma_k^2 + \delta_k^2} \ge \gamma_k, \ \forall k, \tag{16b}$$

$$\eta_k(1-\rho_k)\left(\sum_{l=1}^{K}\boldsymbol{h}_k^H\boldsymbol{V}_{\mathrm{RF}}\boldsymbol{X}_l\boldsymbol{V}_{\mathrm{RF}}^H\boldsymbol{h}_k + \sigma_k^2\right) \ge e_k, \ \forall k, \tag{16c}$$

$$0 < \rho_k < 1. \quad \forall k \tag{16d}$$

$$\boldsymbol{X}_k \succeq \boldsymbol{0}, \quad \mathrm{rank}\{\boldsymbol{X}_k\} = 1, \quad \forall k. \tag{16e}$$

Note that problem (16) is non-convex because of products between ρ_k's and $\boldsymbol{X}_k$'s as well as the rank constraint $\mathrm{rank}\{\boldsymbol{X}_k\} = 1$. By dropping the rank-one constraint and reorganizing terms in each constraint, the SDR of problem (16) is written as

$$\min_{\{\boldsymbol{X}_k,\rho_k\}} \ \mathrm{Tr}(\boldsymbol{V}_{\mathrm{RF}}\sum_{k=1}^{K}\boldsymbol{X}_k\boldsymbol{V}_{\mathrm{RF}}^H) \tag{17a}$$

$$\text{s.t.} \quad \boldsymbol{h}_k^H\boldsymbol{V}_{\mathrm{RF}}\boldsymbol{X}_k\boldsymbol{V}_{\mathrm{RF}}^H\boldsymbol{h}_k - \gamma_k\sum_{l\neq k}^{K}\boldsymbol{h}_k^H\boldsymbol{V}_{\mathrm{RF}}\boldsymbol{X}_l\boldsymbol{V}_{\mathrm{RF}}^H\boldsymbol{h}_k \ge \gamma_k\left(\frac{\delta_k^2}{\rho_k} + \sigma_k^2\right), \quad \forall k, \tag{17b}$$

$$\sum_{l=1}^{K}\boldsymbol{h}_k^H\boldsymbol{V}_{\mathrm{RF}}\boldsymbol{X}_l\boldsymbol{V}_{\mathrm{RF}}^H\boldsymbol{h}_k \ge \frac{e_k}{\eta_k(1-\rho_k)} - \sigma_k^2, \quad \forall k, \tag{17c}$$

$$0 < \rho_k < 1. \quad \forall k \tag{17d}$$

$$\boldsymbol{X}_k \succeq \boldsymbol{0} \quad \forall k. \tag{17e}$$

Problem (17) is now convex. The solution of problem (17), $\{\boldsymbol{X}_k^*, \rho_k^*\}$, can be found by interior-point algorithm using CVX [32]. If $\boldsymbol{X}_k*$ satisfies $\mathrm{rank}\{\boldsymbol{X}_k*\} = 1$, the kth vector of $\boldsymbol{V}_{\mathrm{Dig}}^*$ is obtained by eigenvalue decomposition (EVD) such as $\boldsymbol{V}_{\mathrm{Dig},k}^* = \boldsymbol{U}_k\Sigma_k^{1/2}$ where $\boldsymbol{X}_k^* = \boldsymbol{U}_k\Sigma_k\boldsymbol{U}_k^H$, and $\boldsymbol{V}_{\mathrm{Dig}}^*$ becomes the optimal solution of (16). From the following proposition, it is confirmed that the optimal solution of (16) is always obtained by solving problem (17) when $\mathrm{rank}(\boldsymbol{V}_{\mathrm{RF}}) = N_{\mathrm{RF}}$.

Proposition 1: Assuming $\mathrm{rank}(\boldsymbol{V}_{\mathrm{RF}}) = N_{\mathrm{RF}}$, we have

1) Constraints (17b) and (17c) are satisfied with equality.
2) For problem (17), $\mathrm{rank}(\boldsymbol{X}_k^*) = 1, \forall k$.

Proof: please refer to Appendix B.

The overall proposed algorithm of obtaining digital and analog precoders is summarised in Algorithm 1 which is called OptDig-ProRF scheme. Although we relaxed individual constraints in problem (13), through numerical results, we shall show that the OptDig-ProRF scheme yields practically similar performance to the fully digital beamforming scheme even when $\{e_k\}$ and $\{\gamma_k\}$ are distinct.

IV. HYBRID BEAMFORMING SWIPT WITH ZERO-FORCING DIGITAL PRECODER

If a ZF digital precoder is used instead of the optimal digital precoder, we can further reduce the amount of computational load and searching time to find the solution. In order to make the problem tractable, we first separate the problem into two steps: 1) designing the ZF digital precoder for a given analog precoder; 2) designing a suboptimal analog precoder for a given ZF digital precoder. Then the above two steps are iteratively repeated until the transmit power difference between two consecutive updates falls below a threshold. In the algorithm, one can start with either of the two steps first. While this ZF-based hybrid beamforming requires iterations, due to the closed-form expression of the ZF digital precoder, the computational complexity still can be reduced.

Algorithm 1 OptDig-ProRF Scheme

Require: $\boldsymbol{H}, e_k, \gamma_k, \sigma_k, \delta_k, \eta_k, \forall k$.
Initialize $\boldsymbol{V}_{\mathrm{RF}}$ using CAZAC sequences.
$P_{\mathrm{prev}} \leftarrow \infty$, $P_{\mathrm{current}} \leftarrow \log\left|\boldsymbol{H}\boldsymbol{V}_{\mathrm{RF}}\boldsymbol{V}_{\mathrm{RF}}^{H}\boldsymbol{H}^{H}\right|$.
while $(P_{\mathrm{current}} - P_{\mathrm{prev}})/P_{\mathrm{current}} \geq \epsilon_{\mathrm{th}}$ **do**
  for $i = 1 : N$ **do**
    for $j = 1 : N_{\mathrm{RF}}$ **do**
      Find $\boldsymbol{V}_{\mathrm{RF}}(i,j) = \frac{\chi_{i,j}}{|\chi_{i,j}|}$
    end for
  end for
  $P_{\mathrm{prev}} \leftarrow P_{\mathrm{current}}$, $P_{\mathrm{current}} \leftarrow \log\left|\boldsymbol{H}\boldsymbol{V}_{\mathrm{RF}}\boldsymbol{V}_{\mathrm{RF}}^{H}\boldsymbol{H}^{H}\right|$.
end while
$\boldsymbol{V}_{\mathrm{RF}}^{*} \leftarrow \boldsymbol{V}_{\mathrm{RF}}$.
Find $\boldsymbol{X}_k^{*}$ and $\rho_k^{*}, \forall k$ by solving problem (17).
Find $\boldsymbol{V}_{\mathrm{Dig},k}^{*} = \boldsymbol{U}_k \Sigma_k^{1/2}, \forall k$ where $\boldsymbol{X}_k^{*} = \boldsymbol{U}_k \Sigma_k \boldsymbol{U}_k^{H}$.
Return: $\boldsymbol{V}_{\mathrm{RF}}^{*}, \boldsymbol{V}_{\mathrm{Dig}}^{*}, \rho_k^{*}, \forall k$.

A. ZF DIGITAL PRECODER

Assuming that an analog precoder $\boldsymbol{V}_{\mathrm{RF}}$ is given and the ZF precoder $\boldsymbol{V}_{\mathrm{Dig}}^{\mathrm{ZF}}$ is used, the received signals of all users can be expressed as a vector such as

$$\begin{aligned}\boldsymbol{y} &= \boldsymbol{H}\boldsymbol{V}_{\mathrm{RF}}\boldsymbol{V}_{\mathrm{Dig}}^{\mathrm{ZF}}\boldsymbol{s} + \boldsymbol{n} \\ &= \boldsymbol{P}^{\frac{1}{2}}\boldsymbol{s} + \boldsymbol{n},\end{aligned} \tag{18}$$

where

$$\begin{aligned}\boldsymbol{V}_{\mathrm{Dig}}^{\mathrm{ZF}} &= \boldsymbol{V}_{\mathrm{RF}}^{H}\boldsymbol{H}^{H}(\boldsymbol{H}\boldsymbol{V}_{\mathrm{RF}}\boldsymbol{V}_{\mathrm{RF}}^{H}\boldsymbol{H}^{H})^{-1}\boldsymbol{P}^{\frac{1}{2}}, \\ \boldsymbol{P} &= \mathrm{diag}(p_1, \cdots, p_K).\end{aligned} \tag{19}$$

We can see that finding $\boldsymbol{V}_{\mathrm{Dig}}^{\mathrm{ZF}}$ is reduced to finding $\boldsymbol{P}$. Denoting $\widetilde{\boldsymbol{V}} = \boldsymbol{V}_{\mathrm{RF}}^{H}\boldsymbol{H}^{H}(\boldsymbol{H}\boldsymbol{V}_{\mathrm{RF}}\boldsymbol{V}_{\mathrm{RF}}^{H}\boldsymbol{H}^{H})^{-1}$, we express the transmit power as $\mathrm{Tr}(\widetilde{\boldsymbol{V}}^{H}\boldsymbol{V}_{\mathrm{RF}}^{H}\boldsymbol{V}_{\mathrm{RF}}\widetilde{\boldsymbol{V}}\boldsymbol{P})$ instead of $\mathrm{Tr}(\boldsymbol{V}_{\mathrm{RF}}\boldsymbol{V}_{\mathrm{Dig}}^{\mathrm{ZF}}\boldsymbol{V}_{\mathrm{Dig}}^{\mathrm{ZF}H}\boldsymbol{V}_{\mathrm{RF}}^{H})$, so that $\boldsymbol{P}$ is revealed explicitly in the objective function. The signals split for ID and EH at user k are now expressed as

$$y_k^{\mathrm{ID}} = \sqrt{\rho_k}\left(\sqrt{p_k}s_k + n_k\right) + z_k, \tag{20}$$

$$y_k^{\mathrm{EH}} = \sqrt{1-\rho_k}\left(\sqrt{p_k}s_k + n_k\right), \tag{21}$$

respectively. We can formulate the power-minimization problem whose variables are $\{p_k, \rho_k\}$ as follows

$$\min_{\{p_k,\rho_k\}} \quad \mathrm{Tr}(\widetilde{\boldsymbol{V}}^{H}\boldsymbol{V}_{\mathrm{RF}}^{H}\boldsymbol{V}_{\mathrm{RF}}\widetilde{\boldsymbol{V}}\boldsymbol{P}) \tag{22a}$$

$$\text{s. t.} \quad \frac{\rho_k p_k}{\rho_k\sigma_k^2 + \delta_k^2} \geq \gamma_k, \quad \forall k, \tag{22b}$$

$$\eta_k(1-\rho_k)\left(p_k + \sigma_k^2\right) \geq e_k, \quad \forall k, \tag{22c}$$

$$0 < \rho_k < 1, \quad \forall k. \tag{22d}$$

Problem (22) is non-convex because of products between ρ_k and p_k in (22b) and (22c). We can reformulate the above problem into a convex problem as follows

$$\min_{\{p_k,\rho_k\}} \quad \mathrm{Tr}(\widetilde{\boldsymbol{V}}^{H}\boldsymbol{V}_{\mathrm{RF}}^{H}\boldsymbol{V}_{\mathrm{RF}}\widetilde{\boldsymbol{V}}\boldsymbol{P}) \tag{23a}$$

$$\text{s. t.} \quad p_k \geq \gamma_k\left(\sigma_k^2 + \frac{\delta_k^2}{\rho_k}\right), \quad \forall k, \tag{23b}$$

$$p_k \geq \frac{e_k}{\eta_k(1-\rho_k)} - \sigma_k^2, \quad \forall k, \tag{23c}$$

$$0 < \rho_k < 1, \quad \forall k. \tag{23d}$$

For a given k, the optimal solution of problem (23) can be found as

$$\rho_k^{*} = \frac{-(\alpha_k + \beta_k - 1) + \sqrt{(\alpha_k + \beta_k - 1)^2 + 4\beta_k}}{2}, \tag{24a}$$

$$p_k^{*} = \gamma_k\left(\sigma_k^2 + \frac{\delta_k^2}{\rho_k^{*}}\right), \tag{24b}$$

where $\alpha_k = \frac{e_k}{\eta_k(\gamma_k+1)\sigma^2}$ and $\beta_k = \frac{\gamma_k\delta_k^2}{(\gamma_k+1)\sigma_k^2}$. Detailed proof can be found in Appendix C. By substituting $\{p_k^{*}\}$ into the right-hand-side of (19), $\boldsymbol{V}_{\mathrm{Dig}}^{\mathrm{ZF}}$ is obtained.

B. CORRESPONDING ANALOG PRECODER

We can see that $\boldsymbol{V}_{\mathrm{RF}}$ is involved with problem (23) only through the objective function. Therefore, for a given $\boldsymbol{V}_{\mathrm{ZF}}^{\mathrm{Dig}}$ and ρ_k, the problem for finding analog precoder can be reduced into

$$\min_{\{\boldsymbol{V}_{\mathrm{RF}}\}} \quad f(\boldsymbol{V}_{\mathrm{RF}}) \triangleq \mathrm{Tr}(\widetilde{\boldsymbol{V}}^{H}\boldsymbol{V}_{\mathrm{RF}}^{H}\boldsymbol{V}_{\mathrm{RF}}\widetilde{\boldsymbol{V}}\boldsymbol{P}) \tag{25a}$$

$$|\boldsymbol{V}_{\mathrm{RF}}(i,j)|^2 = 1, \quad \forall i,j. \tag{25b}$$

Soharbi and Yu [22] also dealt with the same problem as (25), so that we also apply their solution here. They proposed to approximate the utility function of problem (25) into $\hat{f}(\boldsymbol{V}_{\mathrm{RF}})$ assuming $N_{\mathrm{RF}} > K$ and a very large N, then adjust the angle of $\boldsymbol{V}_{\mathrm{RF}}(i,j)$ minimizing $\hat{f}(\boldsymbol{V}_{\mathrm{RF}})$ by maintaining rest elements of $\boldsymbol{V}_{\mathrm{RF}}$, i.e.,

$$\theta_{i,j}^{ZF*} = \arg\min_{\theta_{i,j}} \hat{f}(\theta_{i,j}). \tag{26}$$

The closed-form solution of problem (26) was obtained and we encourage the readers to refer to Section V-B of [22] for the solution and detailed information. When problem (26) is solved for all i, j, we consider $\boldsymbol{V}_{\mathrm{RF}}$ to have been updated once. This can be repeated until $\boldsymbol{V}_{\mathrm{RF}}$ converges. Overall, updating of $\boldsymbol{V}_{\mathrm{RF}}$ and $(\boldsymbol{P}, \rho_k)$ continues until f converges. The whole process is summarised in Algorithm 2 which is called ZfDig-SohRF scheme.

V. SIMULATIONS

A. CHANNEL MODEL

For simulations, we use the geometric channel model applied in [33] which also considered hybrid precoding for massive multiuser MIMO systems. Assuming a uniform linear array (ULA) antenna configuration at the BS, the channel vector from the BS to the kth user is given by

$$\boldsymbol{h}_k^{H} = \sqrt{\frac{N}{L}}\sum_{l=1}^{L}\alpha_k^{l}\boldsymbol{a}(\phi_k^{l})^{H}, \tag{27}$$

Algorithm 2 ZfDig-SorRF Scheme

Require: $\boldsymbol{H}, e_k, \gamma_k, \sigma_k, \delta_k, \eta_k, \forall k$.

Initialize $\boldsymbol{P} \leftarrow \boldsymbol{I}_K, \boldsymbol{V}_{\mathrm{RF}}$ using CAZAC sequences.
$P^{\mathrm{out}}_{\mathrm{prev}} \leftarrow \infty, P^{\mathrm{out}}_{\mathrm{current}} \leftarrow f(\boldsymbol{V}_{\mathrm{RF}}, \boldsymbol{P})$.
while $(P^{\mathrm{out}}_{\mathrm{prev}} - P^{\mathrm{out}}_{\mathrm{current}})/P^{\mathrm{out}}_{\mathrm{current}} \geq \epsilon^{\mathrm{out}}_{\mathrm{th}}$ **do**
  $P^{\mathrm{in}}_{\mathrm{prev}} \leftarrow \infty, P^{\mathrm{in}}_{\mathrm{current}} \leftarrow \hat{f}(\boldsymbol{V}_{\mathrm{RF}}, \boldsymbol{P})$.
  while $(P^{\mathrm{in}}_{\mathrm{prev}} - P^{\mathrm{in}}_{\mathrm{current}})/P^{\mathrm{in}}_{\mathrm{current}} \geq \epsilon^{\mathrm{in}}_{\mathrm{th}}$ **do**
    for $i = 1 : N$ **do**
      for $j = 1 : N_{\mathrm{RF}}$ **do**
        Find $\angle \boldsymbol{V}_{\mathrm{RF}}(i,j) = \arg\min_{\theta_{i,j}} \hat{f}(\theta_{i,j})$
      end for
    end for
    $P^{\mathrm{in}}_{\mathrm{prev}} \leftarrow P^{\mathrm{in}}_{\mathrm{current}}, P^{\mathrm{in}}_{\mathrm{current}} \leftarrow \hat{f}(\boldsymbol{V}_{\mathrm{RF}}, \boldsymbol{P})$.
  end while
  Find p^*_k and $\rho^*_k \forall k$ from problem (24).
  $\boldsymbol{P} \leftarrow \mathrm{diag}(p^*_1, \cdots, p^*_K)$
  $P^{\mathrm{out}}_{\mathrm{prev}} \leftarrow P^{\mathrm{out}}_{\mathrm{current}}, P^{\mathrm{out}}_{\mathrm{current}} \leftarrow f(\boldsymbol{V}_{\mathrm{RF}}, \boldsymbol{P})$
end while
$\boldsymbol{V}^{\mathrm{ZF}}_{\mathrm{Dig}} \leftarrow \boldsymbol{V}^H_{\mathrm{RF}} \boldsymbol{H}^H (\boldsymbol{H}\boldsymbol{V}_{\mathrm{RF}}\boldsymbol{V}^H_{\mathrm{RF}}\boldsymbol{H}^H)^{-1}\boldsymbol{P}^{\frac{1}{2}}$
$\boldsymbol{V}^*_{\mathrm{RF}} \leftarrow \boldsymbol{V}_{\mathrm{RF}}$

Return: $\boldsymbol{V}^*_{\mathrm{RF}}, \boldsymbol{V}^{\mathrm{ZF}}_{\mathrm{Dig}}, \rho^*_k \forall k$.

where L denote the number of propagation paths, $\alpha^l_k \sim \mathcal{CN}(0, \omega_k)$ denotes the complex gain of the lth path to the kth user, $\phi_k \in [0, 2\pi)$ is the random angle of departure, ω_k is the variance of channel gains of the kth user. And $\boldsymbol{a}(\phi)$ is the array response vector of the ULA antenna written as

$$\boldsymbol{a}(\phi) = \frac{1}{\sqrt{N}} \left[1, e^{\frac{j2\pi\tilde{d}\sin(\phi)}{\lambda}}, \cdots, e^{\frac{j2\pi d(N-1)\sin(\phi)}{\lambda}}\right]^T, \quad (28)$$

where λ is the wavelength and $\tilde{d}$ is the normalized antenna spacing. In numerical examples, $\tilde{d} = \lambda/2$ and $L = 15$ are considered. All the numerical results are obtained using Monte-Carlo simulations over more than 2,000 channel realizations.

B. INDIVIDUALLY DIFFERENT CONSTRAINTS AND PATH-LOSS

We illustrate the results for a scenario where users have different path-losses ($1/\omega_k$), SINR constraints, and energy constraints, to observe how the proposed schemes work under individual constraints. Every channel realization, we randomly generate γ_k, e_k, and ω_k values whose dB-scaled values follow uniform distributions such as $10\log_{10}(\gamma_k) \sim \mathcal{U}(\bar{\gamma}_{dB} - d_\gamma, \bar{\gamma}_{dB} + d_\gamma)$, $10\log_{10}(e_k) \sim \mathcal{U}(\bar{e}_{dB} - d_e, \bar{e}_{dB} + d_e)$ and $10\log_{10}(\omega_k) \sim \mathcal{U}(\bar{\omega}_{dB} - d_\omega, \bar{\omega}_{dB} + d_\omega)$, respectively. Here, $\bar{\gamma}_{dB}, \bar{e}_{dB}$, and $\bar{\omega}_{dB}$ denote mean values of dB-scaled γ_k, e_k, and ω_k, respectively, and $\mathcal{U}(a, b)$ denotes a uniform distribution between a and b. In all simulations, the antenna noise variance, additional noise variance and energy transfer efficiency are set identically as $\sigma^2 = -70$ dBm, $\delta^2 = -50$ dBm, and $\eta = 0.5$. Moreover, we use $d_\gamma = 4, d_e = 4, \bar{\omega}_{\mathrm{dB}} - 40$ dB, and $d_\omega = 10$ unless otherwise noted. Each user has its path-loss uniformly distributed in $[-50, -30]$ dB which corresponds to the distance ranging from 0.94m to 9.4m in free space when the carrier frequency is 800 MHz.

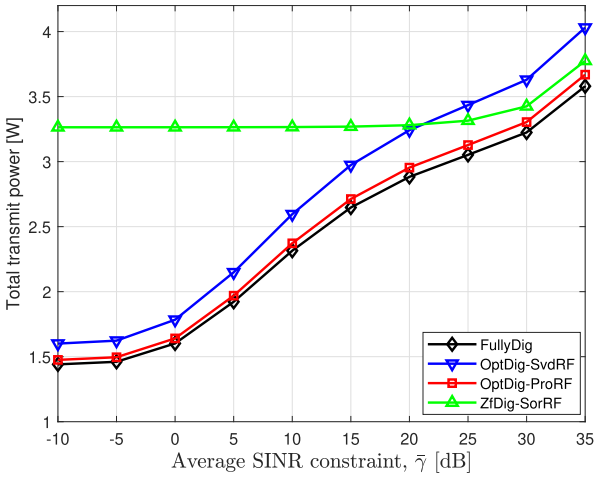

FIGURE 1. Transmission power [W] vs. $\bar{\gamma}$ [dB] when $K = 8$, $N_{\mathrm{RF}} = 16$, $N = 32$, $\bar{e}_{\mathrm{dB}} = -10$ dBm, and $\bar{\omega}_{\mathrm{dB}} = -40$ dB.

C. CONVENTIONAL ANALOG PRECODING SCHEME

As a conventional analog precoding scheme, we consider a singular value decomposition (SVD) based analog precorder which was used in [28]. The SVD of channel $\boldsymbol{H}$ is written as

$$\boldsymbol{H} = \boldsymbol{U}\Sigma\boldsymbol{V}^{\mathrm{H}}, \quad (29)$$

where $\boldsymbol{U}$ and $\boldsymbol{V}$ denote the left- amd right- singular vectors. Then, each element in $\boldsymbol{V}_{\mathrm{RF}}$ is chosen as

$$\boldsymbol{V}_{\mathrm{RF}}(i,j) = \frac{\boldsymbol{V}(i,j)}{|\boldsymbol{V}(i,j)|}, \quad i \in \{1, \cdots, N\}, j \in \{1, \cdots, N_{\mathrm{RF}}\}. \quad (30)$$

Let the OptDig-SvdRF scheme denote a hybrid beamforming design whose digital precoder is obtained by solving problem (17) and analog precoder based on the SVD.

D. ILLUSTRATIVE RESULTS

We used the following convention for labeling the curves in the plots: X-Y, where X denotes the digital precoding method (FullyDig: fully digital, OptDig: optiaml digital, ZfDig: ZF digital), Y denotes analog precoding method (ProRF: proposed precoder, SohRF: analog precoder in [22], SvdRF: SVD based analog precoder).

Fig. 1 shows the transmission power versus the average SINR constraint, $\bar{\gamma}$, for *FullyDig*, *OptDig-ProRF*, *ZfDig-SohRF*, and *OptDig-SvdRF* schemes with $K = 8$, $N_{\mathrm{RF}} = 16$, $N = 32$, $\bar{e}_{\mathrm{dB}} = -10$ dBm, $\bar{\omega}_{\mathrm{dB}} = -40$ dB. The transmit power of all schemes but *ZfDig-SohRF* increases as the value of $\bar{\gamma}$ increases. The performance of *OptDig-ProRF* is practically similar to that of *FullyDig* for whole values of $\bar{\gamma}$. The *OptDig-SvdRF* scheme exhibits higher transmit power consumption compared to *FullyDig* and *OptDig-ProRF* as $\bar{\gamma}$ increases from -10 to 35 dB. For instance, at $\bar{\gamma} = -10$ dB

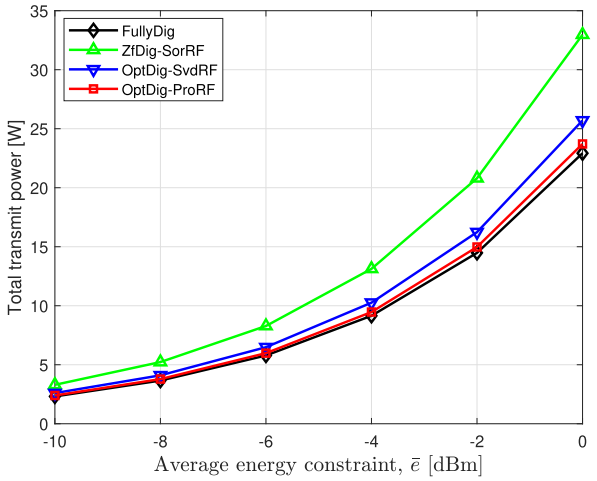

FIGURE 2. Transmission power [W] vs. $\bar{e}$ [dB] when $K = 8$, $N_{\mathrm{RF}} = 16$, $N = 32$, $\bar{\gamma}_{\mathrm{dB}} = 10$ dB, and $\bar{\omega}_{\mathrm{dB}} = -40$ dB.

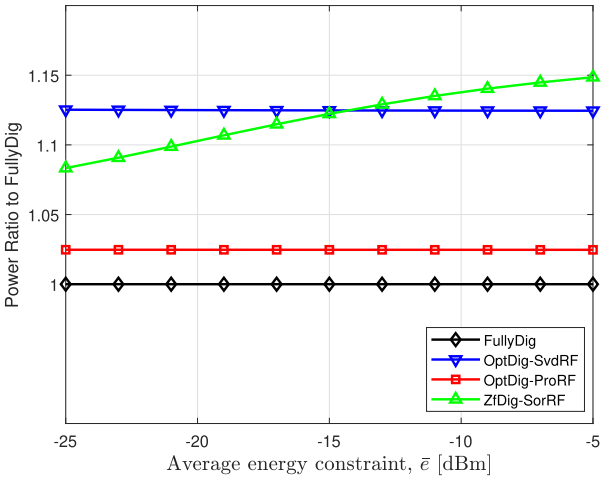

FIGURE 3. Transmission power ratio vs. $\bar{e}$ [dB] when $K = 8$, $N_{\mathrm{RF}} = 16$, $N = 32$, $\bar{\gamma}_{\mathrm{dB}} = 20$ dB, and $\bar{\omega}_{\mathrm{dB}} = -40$ dB.

and $\bar{\gamma} = 35$ dB, *OptDig-ProRF* utilizes 92% and 91% of the transmit power consumed by *OptDig-SvdRF*, respectively. This reduction in power consumption solely stems from the proposed analog precoder design outlined in Algorithm 1. Interestingly, the transmit power of *ZfDig-SohRF* shows only a marginal increase as $\bar{\gamma}$ increases from -5 to 25 dB, while it experiences a notable increase from 30 to 35 dB. The ZF-based digital precoder always eliminates inter-user interference, leading the BS to increase the transmit power in order to satisfy the dominant constraints which could be energy or SINR constraints depending on situations. When the value of $\bar{\gamma}$ is small, implying that energy constraints are dominant, the transmit power level of *ZfDig-SohRF* is primarily determined by $\bar{e}$ rather than $\bar{\gamma}$. Conversely, if $\bar{\gamma}$ has larger values, with SINR constraints becoming dominant, the transmit power level increases as $\bar{\gamma}$ increases. In contrast, both *OptDig-SvdRF* and *OptDig-SvdRF* can flexibly change the level of inter-user interference. For instance, when energy constraints are dominant, the two schemes amplify inter-user interference to extract a larger amount of energy from the received signals. This difference between ZF-based digital precoding and optimal digital precoding causes the observed gap in power consumption. In addition, *ZfDig-SohRF* exhibits superior performance compared to *OptDig-SvdRF* for $\bar{\gamma} \geq 25$ and converges towards the performance of both *OptDig-ProRF* and *FullyDig* for $\bar{\gamma} \geq 30$. These arise due to the superiority of the analog precoder proposed in [22] over the SVD-based analog precoder, and minimizing inter-user interference is close to optimality under high SINR constraints.

Fig. 2 displays the transmission power versus $\bar{e}$ for various hybrid beamforming schemes when $K = 8$, $N_{\mathrm{RF}} = 16$, $N = 32$, $\bar{\gamma}_{\mathrm{dB}} = 10$ dB, and $\bar{\omega}_{\mathrm{dB}} = -40$ dB. We can observe that the transmit power of all schemes increases as the value of $\bar{e}$ increases. The *OptDig-ProRF* scheme outperforms the *OptDig-SvdRF* and yields similar performance to that

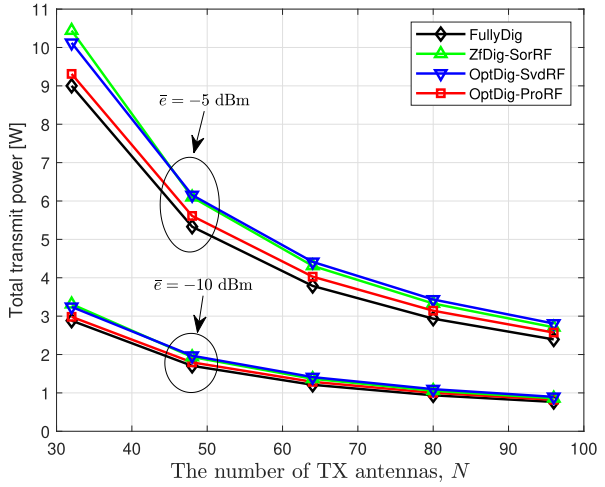

FIGURE 4. Transmission power [W] vs. N for $\bar{e}_{\mathrm{dB}} = -5$ and -10 dBm when $K = 8$, $N_{\mathrm{RF}} = 16$, $\bar{\gamma}_{\mathrm{dB}} = 20$ dB, and $\bar{\omega}_{\mathrm{dB}} = -40$ dB.

of *FullyDig*. As an example, *OptDig-ProRF* utilizes 92% of the transmit power consumed by *OptDig-SvdRF* while using 103% of the transmit power consumed by *FullyDig* when $\bar{e} = 0$ dBm. The *ZfDig-SohRF* scheme shows significant performance degradation compared to the other three schemes. This phenomenon arises due to the fact that the range of $\bar{e}$ considered in Fig. 2 makes energy constraints dominant.

Fig. 3 describes the transmission power ratio of each scheme to *FullyDig* as $\bar{e}$ varies, with parameters $K = 8$, $N_{\mathrm{RF}} = 16$, $N = 32$, $\bar{\gamma}_{\mathrm{dB}} = 20$ dB, and $\bar{\omega}_{\mathrm{dB}} = -40$ dB. We can observe that the ratios for *OptDig-ProRF* and *OptDig-SvdRF* do not change with respect to $\bar{e}$. However, as $\bar{e}$ increases, it can be noted that the power of *ZfDig-SorRF* increases at a higher rate compared to that of *FullyDig*. This result is consistent with the performance degradation of *ZfDig-SorRF* when energy constraint are dominant as shown in Fig. 1 and Fig. 2.

Fig. 4 depicts the transmission power versus N for $\bar{e}_{\mathrm{dB}} = -5$ and -10 dBm, while maintaining constant values

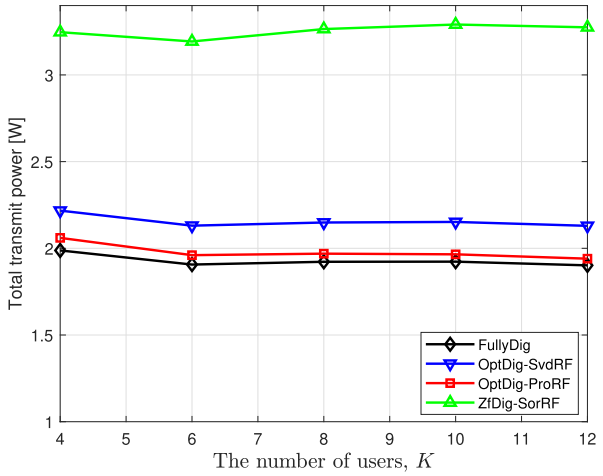

FIGURE 5. Transmission power [W] vs. K with $N_{\mathrm{RF}} = 2K$ and $N = 4K$ when $\bar{\gamma}_{\mathrm{dB}} = 5$ dB, $\bar{e}_{\mathrm{dB}} = -10$dBm, and $\bar{\omega}_{\mathrm{dB}} = -40$ dB.

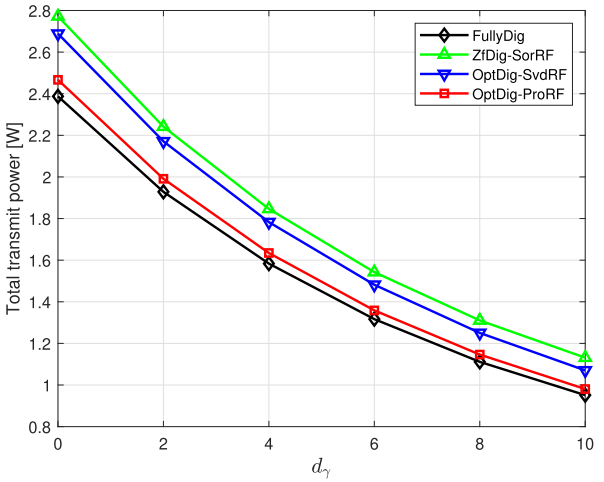

FIGURE 6. Transmission power [W] vs. d_γ when $K = 8$, $N_{\mathrm{RF}} = 16$, $N = 32$, $\bar{\gamma}_{\mathrm{dB}} = 20$ dB, $\bar{e}_{\mathrm{dB}} = -5$dBm, and $\bar{\omega}_{\mathrm{dB}} = -40$ dB.

of $K = 8$ and $N_{\mathrm{RF}} = 16$, when $\bar{\gamma}_{\mathrm{dB}} = 20$ dB and $\bar{\omega}_{\mathrm{dB}} = -40$ dB. We can observe that the transmit power of all schemes decreases as N increases. For example, in the case of *OptDig-ProRF*, when N doubles from 32 to 64, the transmit power decreases by 57%, going from 9.3 W to 4.0 W for $\bar{e}_{\mathrm{dB}} = -5$ dB. This observation demonstrates the advantageous impact of employing a larger antenna array. The performance of *OptDig-ProRF* closely matches that of *FullyDig* across all values of N, thereby confirming the superiority of the proposed scheme.

Fig. 5 illustrates the relationship between transmission power and K, while ensuring that the values of N_{RF} and N vary proportionally to N, namely $N_{\mathrm{RF}} = 2K$ and $N = 4K$. This is observed when $\bar{\gamma}_{\mathrm{dB}} = 5$ dB, $\bar{e}_{\mathrm{dB}} = -10$dBm, and $\bar{\omega}_{\mathrm{dB}} = -40$ dB. We can observe that the transmit power of all schemes remains nearly consistent despite variations in K, as long as K, N_{RF}, and N maintain proportional relationships. The performance differences among the beamforming schemes are observed to be similar to those depicted in Fig. 1 at $\bar{\gamma} = 5$ dB.

Fig. 6 depicts the transmission power versus d_γ when $K = 8$, $N_{\mathrm{RF}} = 16$, $N = 32$ $\bar{\gamma}_{\mathrm{dB}} = 20$ dB, $\bar{e}_{\mathrm{dB}} = -5$dBm, and $\bar{\omega}_{\mathrm{dB}} = -40$ dB. It can be observed that when SINR constraints for each user are widely distributed, the transmit power decreases. All schemes exhibit a similar performance trend as shown in Fig. 4. Importantly, *OptDig-ProRF* consumes nearly the same transmit power as *FullyDig*, even when $d_\gamma = 10$, indicating that the values of γ_k are uniformly distributed within a 20 dB range.

Fig. 7 describes the transmission power versus $\bar{\gamma}$ for various values of N_{RF} when $K = 8, N = 32, \bar{e}_{\mathrm{dB}} = -5$ dBm, and $\bar{\omega}_{\mathrm{dB}} = -40$ dB. In this simulation, 1,000 channel realizations are used with $L = 15$. We can observe that the transmit power decreases as N_{RF} increases, for example, transmit powers are 7.34, 7.07, 6.94 W for $N_{\mathrm{RF}} = 8, 12, 16$ at $\bar{\gamma} = 10$ dB, which are 108%, 104%, 102% of the transmit power of *FullyDig*.

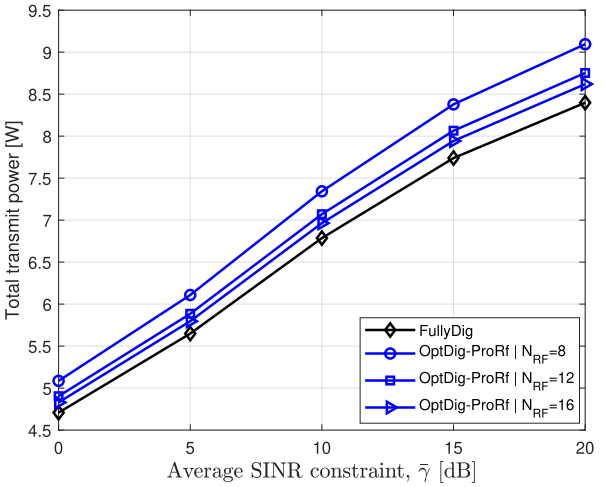

FIGURE 7. Transmission power [W] vs. $\bar{\gamma}$ [dB] for various values of N_{RF} when $K = 8$, $N = 32$, $\bar{e}_{\mathrm{dB}} = -5$ dBm, and $\bar{\omega}_{\mathrm{dB}} = -40$ dB.

E. COMPLEXITY ANALYSIS

We assume that the multiplication between an $m \times p$ matrix and a $p \times n$ matrix has a time complexity of $\mathcal{O}(mpn)$, and the complexities of computing the inverse and determinant of an $n \times n$ matrix are both $\mathcal{O}(n^3)$. Referring to [34], the computation load of *FullyDig*, which solves problem (8) with the interior-point algorithm, is known as $\mathcal{O}(\sqrt{KN}(K^3N^2 + K^2N^3))$.

In *OptDig-ProRF*, the digital and analog precoders are obtained separately. To obtain the digital precoder (steps 12 to 13), we need to solve the problem (17) with the interior-point algorithm and it introduces a complexity of $\mathcal{O}(\sqrt{KN_{\mathrm{RF}}}(K^3N_{\mathrm{RF}}^2 + K^2N_{\mathrm{RF}}^3))$, which is interestingly independent of N. On the other hand, for the analog precoder, we need to calculating $\chi_{i,j}$ which involves several matrix products with a complexity of $\mathcal{O}(NN_{\mathrm{RF}}K)$ and the calculation is repeated NN_{RF} times. Therefore, the complexity of *OptDig-ProRF* can be expressed as $\mathcal{O}(N^2N_{\mathrm{RF}}^2K) + \mathcal{O}(\sqrt{KN_{\mathrm{RF}}}(K^3N_{\mathrm{RF}}^2 + K^2N_{\mathrm{RF}}^3))$. Meanwhile, since the time

TABLE 1. Complexities of various schemes under different assumptions.

schemes	$N \gg N_{\mathrm{RF}}$ $N \gg K$	$N \propto N_{\mathrm{RF}}$ $N \gg K$	$N \propto N_{\mathrm{RF}}$ $N \propto K$
FullyDig	$\mathcal{O}(N^{3.5})$	$\mathcal{O}(N^{3.5})$	$\mathcal{O}(N^6)$
OptDig-ProRF	$\mathcal{O}(N^2)$	$\mathcal{O}(N^4)$	$\mathcal{O}(N^6)$
ZFDig-SorRF	$\mathcal{O}(N^2)$	$\mathcal{O}(N^4)$	$\mathcal{O}(N^5)$
OptDig-SvdRF	$\mathcal{O}(N)$	$\mathcal{O}(N^{3.5})$	$\mathcal{O}(N^6)$

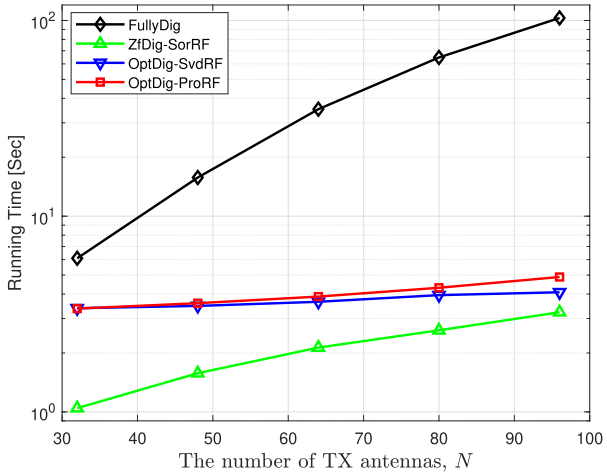

FIGURE 8. Average running time [Sec] vs. N when $K = 8$, $N_{\mathrm{RF}} = 16$, $\bar{e}_{\mathrm{dB}} = -10$ dBm, $\bar{\gamma}_{\mathrm{dB}} = 20$ dB, and $\bar{\omega}_{\mathrm{dB}} = -40$ dB.

complexity of the singular value decomposition (SVD) of an $m \times n$ matrix is $\mathcal{O}(mn\min(m,n))$ [35], the complexity of *OptDig-SvdRF* is expressed as $\mathcal{O}(NN_{\mathrm{RF}}^2) + \mathcal{O}(\sqrt{KN_{\mathrm{RF}}}(K^3N_{\mathrm{RF}}^2 + K^2N_{\mathrm{RF}}^3))$.

In *ZFDig-SorRF*, adjustments of the analog and digital precoders are executed sequentially and repeated until the utility converges in the outer while loop (steps 4 to 16). The analog precoding is run in the inner while loop (steps 5 to 10), and step 8 is repeated NN_{RF} times in the loop. Step 8 is executed by calculating the closed-form expressions in Section V-B of [22], whose complexity is $\mathcal{O}(NN_{\mathrm{RF}}K)$. The primary step of the digital process (step 13) is executed by calculating the closed-form expression, whose complexity is known as $\mathcal{O}(K^4 + K^2N_{\mathrm{RF}}^2)$. In this respect, we can express the computational load of *ZFDig-SorRF* as $\mathcal{O}(N^2N_{\mathrm{RF}}^2K) + \mathcal{O}(K^4 + K^2N_{\mathrm{RF}}^2)$ [11].

Table 1 summarizes the complexities of various schemes under three different assumptions: i) $N \gg N_{\mathrm{RF}}$ and $N \gg K$; ii) $N \propto N_{\mathrm{RF}}$ and $N \gg K$; iii) $N \propto N_{\mathrm{RF}}$ and $N \propto K$. Note that it is assumed that the number of iterations in while loops is negligible compared to N, N_{RF}, and K. Under the first assumption, which is closest to the practical scenarios, we can see that the proposed schemes have a lower order of complexity than that of *FullyDig* in terms of N. When N, N_{RF}, and N_{RF} increase proportionally, *ZFDig-SorRF* has a lower order of complexity than *OptDig-ProRF*.

Fig. 8 shows the average running time [Sec] vs. N [dB] when $K = 8$, $N_{\mathrm{RF}} = 16$, $\bar{e}$dB $= -5$ dBm, and $\bar{\omega}$dB $= -40$ dB where 100 channel realizations are used. We can observe that the average running time of *FullyDig* increases faster than those of other schemes as N increases. The average running time of *ZFDig-SorRF* is the shortest among the four schemes considered.

VI. CONCLUSION

We considered a hybrid analog-digital precoding-based SWIPT system where a BS with massive transmit antennas transmits to multiple single-antenna users. We aim to minimize transmit-power while guaranteeing harvested energy and SINR requirements of each user. We proposed two suboptimal solutions in which digital and analog precoders are designed separately. In *OptDig-ProRF* scheme, the analog precoder is first found by letting the objective function independent from the digital precoder and power splitting ratios through approximation and finding its local minimum, then the optimal digital precoder and power splitting ratios are found for the obtained analog precoder using semidefinite relaxation. In the *ZfDig-SohRF* scheme, a suboptimal analog precoder is obtained for an initialized digital precoder, then the ZF digital precoder is found for a obtained analog precoder. The two precoders are iteratively found until the transmit power difference between two consecutive updates falls below a threshold. Illustrative results show that the performance of *OptDig-ProRF* is practically similar to that of *FullyDig* for most environments and *ZfDig-SohRF* converges towards the performance of both *OptDig-ProRF* and *FullyDig* when $\bar{\gamma}$ is so high that SINR constraints become dominant. Since the SWIPT system is considered as a promising technology candidate in standard organizations such as ITU and 3GPP, our work may help industry to accelerate the deployment of zero-energy devices in the future. Moreover, integrating our work with the promising non-orthogonal multiple access (NOMA) or rate splitting multiple access (RSMA) techniques could be an interesting and challenging future research topic which deserves comprehensive study.

APPENDIX A

A. DERIVATION OF (14)

The utility function of problem (13) without log() can be written as

$$\begin{aligned}
&\det\left(\boldsymbol{H}\boldsymbol{V}_{\mathrm{RF}}\boldsymbol{V}_{\mathrm{RF}}^H\boldsymbol{H}^H\right) \\
&\quad= \det\left(\boldsymbol{H}\bar{\boldsymbol{V}}_{\mathrm{RF}}^{(j)}\bar{\boldsymbol{V}}_{\mathrm{RF}}^{(j)H}\boldsymbol{H}^H + \boldsymbol{H}\boldsymbol{V}_{\mathrm{RF},j}{\boldsymbol{V}_{\mathrm{RF},j}}^H\boldsymbol{H}^H\right) \\
&\quad= \det\left(\boldsymbol{A}^{(j)} + \boldsymbol{H}\boldsymbol{V}_{\mathrm{RF},j}{\boldsymbol{V}_{\mathrm{RF},j}}^H\boldsymbol{H}^H\right) \qquad \text{(A.1a)} \\
&\quad= \det(\boldsymbol{A}^{(j)}) + {\boldsymbol{V}_{\mathrm{RF},j}}^H\boldsymbol{H}^H\mathrm{adj}(\boldsymbol{A}^{(j)})\boldsymbol{H}\boldsymbol{V}_{\mathrm{RF},j} \qquad \text{(A.1b)}
\end{aligned}$$

where $\bar{\boldsymbol{V}}_{\mathrm{RF}}^{(j)}$ is the sub-matrix of $\boldsymbol{V}_{\mathrm{RF}}$ with the jth column eliminated, $\boldsymbol{A}^{(j)} = \boldsymbol{H}\bar{\boldsymbol{V}}_{\mathrm{RF}}^{(j)}\bar{\boldsymbol{V}}_{\mathrm{RF}}^{(j)H}\boldsymbol{H}^H$, and $\mathrm{adj}(\boldsymbol{A}^{(j)})$ denotes the adjugate matrix of $\boldsymbol{A}^{(j)}$. Eq. (A.1b) is written using the matrix determinant lemma. Using the expression

$$\boldsymbol{H}\boldsymbol{V}_{\mathrm{RF},j} = \bar{\boldsymbol{H}}^{(i)}\bar{\boldsymbol{V}}_{\mathrm{RF},j}^{(i)} + \boldsymbol{h}_i\boldsymbol{V}_{\mathrm{RF}}(i,j) \qquad \text{(A.2)}$$

where $\bar{\boldsymbol{H}}^{(i)}$ is the sub-matrix of $\boldsymbol{H}$ with the ith column eliminated and $\bar{\boldsymbol{V}}_{\mathrm{RF},j}^{(i)}$ is the sub-vector of $\boldsymbol{V}_{\mathrm{RF},j}$ with the ith element

eliminated, the second term in (A.1b) can be written as

$$\begin{aligned} &\boldsymbol{V}_{\mathrm{RF},j}{}^{H}\boldsymbol{H}^{H}\mathrm{adj}(\boldsymbol{A}^{(j)})\boldsymbol{H}\boldsymbol{V}_{\mathrm{RF},j} \\ &\quad = \zeta_{i,j} + 2\mathrm{Re}\left\{\eta_{i,j}\boldsymbol{V}_{\mathrm{RF}}(i,j)\right\} + \kappa_{i,j} \end{aligned} \tag{A.3}$$

where

$$\begin{aligned} \zeta_{i,j} &= (\bar{\boldsymbol{V}}^{(i)}_{\mathrm{RF},j})^{H}(\bar{\boldsymbol{H}}^{(i)})^{H}\mathrm{adj}(\boldsymbol{A}^{(j)})\bar{\boldsymbol{H}}^{(i)}\bar{\boldsymbol{V}}^{(i)}_{\mathrm{RF},j} \\ \chi_{i,j} &= (\bar{\boldsymbol{V}}^{(i)}_{\mathrm{RF},j})^{H}(\bar{\boldsymbol{H}}^{(i)})^{H}\mathrm{adj}(\boldsymbol{A}^{(j)})\boldsymbol{h}_i \\ \kappa_{i,j} &= \boldsymbol{h}_i^{H}\mathrm{adj}(\boldsymbol{A}^{(j)})\boldsymbol{h}_i, \end{aligned} \tag{A.4}$$

and we used the fact that $\mathrm{adj}(\boldsymbol{A}^{(j)})$ is Hermitian matrix since it is an adjugate matrix of Hermitian matrix. Note that $\det(\boldsymbol{A}^{(j)})$, $\zeta_{i,j}$, $\chi_{i,j}$, and $\kappa_{i,j}$, are not dependent on $\boldsymbol{V}_{\mathrm{RF}}(i,j)$. Therefore, the only term dependent on $\boldsymbol{V}_{\mathrm{RF}}(i,j)$ in (A.1b) is $2\mathrm{Re}\left\{\chi_{i,j}\boldsymbol{V}_{\mathrm{RF}}(i,j)\right\}$. Therefore, the angle of $\boldsymbol{V}_{\mathrm{RF}}(i,j)$ to maximize $\det\left(\boldsymbol{H}\boldsymbol{V}_{\mathrm{RF}}\boldsymbol{V}_{\mathrm{RF}}^{H}\boldsymbol{H}^{H}\right)$ is $-\angle\chi_{i,j}$.

APPENDIX B

B. PROOF OF PROPOSITION 1

In [11], the authors showed that, for the fully digital beamforming case, the optimal solution to the semidefinite relaxation version of the power minimization problem expressed as (8) is also the optimal solution to problem (8). We extend the proof to the hybrid precoding case.

Because problem (17) is convex, the optimal duality gap is zero, assuming (17) satisfies Slater's condition. The partial Lagrangian of problem (17) is given by

$$\begin{aligned} &L(\boldsymbol{X}_k, \rho_k, \lambda_k, \nu_k) \\ &\triangleq \mathrm{Tr}(\boldsymbol{V}_{\mathrm{RF}}\sum_{k=1}^{K}\boldsymbol{X}_k\boldsymbol{V}_{\mathrm{RF}}^{H}) \\ &\quad - \sum_{k=1}^{K}\lambda_k\left\{\frac{1}{\gamma_k}\boldsymbol{h}_k^{H}\boldsymbol{V}_{\mathrm{RF}}\boldsymbol{X}_k\boldsymbol{V}_{\mathrm{RF}}^{H}\boldsymbol{h}_k - \sum_{l\neq k}^{K}\boldsymbol{h}_k^{H}\boldsymbol{V}_{\mathrm{RF}}\boldsymbol{X}_l\boldsymbol{V}_{\mathrm{RF}}^{H}\boldsymbol{h}_k\right. \\ &\quad \left. - \left(\frac{\delta_k^2}{\rho_k} + \sigma_k^2\right)\right\} \\ &\quad - \sum_{k=1}^{K}\nu_k\left\{\sum_{l=1}^{K}\boldsymbol{h}_k^{H}\boldsymbol{V}_{\mathrm{RF}}\boldsymbol{X}_l\boldsymbol{V}_{\mathrm{RF}}^{H}\boldsymbol{h}_k - \frac{e_k}{\eta_k(1-\rho_k)} + \sigma_k^2\right\} \end{aligned} \tag{B.1}$$

where we introduce multipliers $\lambda_k \geq 0$ for the K SINR constraints and multipliers $\nu_k \geq 0$ for the K harvest energy constraints. The Lagrangian can be rewritten by

$$\begin{aligned} &L(\boldsymbol{X}_k, \rho_k, \lambda_k, \nu_k) \\ &= \sum_{k=1}^{K}\mathrm{Tr}(\boldsymbol{A}_k\boldsymbol{X}_k) \\ &\quad + \sum_{k=1}^{K}(\lambda_k - \nu_k)\sigma_k^2 + \sum_{k=1}^{K}\left(\frac{\lambda_k\sigma_k^2}{\rho_k} + \frac{\nu_k e_k}{\eta_k(1-\rho_k)}\right) \end{aligned} \tag{B.2}$$

where

$$\begin{aligned} \boldsymbol{A}_k &= \boldsymbol{V}_{\mathrm{RF}}^{H}\boldsymbol{V}_{\mathrm{RF}} + \sum_{l=1}^{K}(\lambda_l - \nu_l)\boldsymbol{V}_{\mathrm{RF}}^{H}\boldsymbol{h}_l\boldsymbol{h}_l^{H}\boldsymbol{V}_{\mathrm{RF}} \\ &\quad - \left(\frac{\lambda_k}{\gamma_k} + \lambda_k\right)\boldsymbol{V}_{\mathrm{RF}}^{H}\boldsymbol{h}_k\boldsymbol{h}_k^{H}\boldsymbol{V}_{\mathrm{RF}}. \end{aligned} \tag{B.3}$$

The dual function is given by

$$g(\lambda, \nu) = \min_{\boldsymbol{X}_k\geq 0, 0<\rho_k<1, \forall k} L(\boldsymbol{X}_k, \rho_k, \lambda_k, \nu_k). \tag{B.4}$$

We define

$$\begin{aligned} \boldsymbol{A}_k^{*} &= \boldsymbol{V}_{\mathrm{RF}}^{H}\boldsymbol{V}_{\mathrm{RF}} + \sum_{l=1}^{K}(\lambda_l^{*} - \nu_l^{*})\boldsymbol{V}_{\mathrm{RF}}^{H}\boldsymbol{h}_l\boldsymbol{h}_l^{H}\boldsymbol{V}_{\mathrm{RF}} \\ &\quad - \left(\frac{\lambda_k^{*}}{\gamma_k} + \lambda_k^{*}\right)\boldsymbol{V}_{\mathrm{RF}}^{H}\boldsymbol{h}_k\boldsymbol{h}_k^{H}\boldsymbol{V}_{\mathrm{RF}}. \end{aligned} \tag{B.5}$$

where $\{\lambda_k^{*}, \nu_k^{*}\} = \arg\max_{\lambda_k, \nu_k \forall k} g(\lambda, \nu)$ are the dual optimal. By substituting these dual optimal into (B.2), the primal optimal which maximizes (B.2) can be obtained by solving following problems separately for given k,

$$\min_{\boldsymbol{X}_k\geq 0} \mathrm{Tr}(\boldsymbol{A}_k^{*}\boldsymbol{X}_k), \tag{B.6}$$

$$\min_{0<\rho_k<1} \frac{\lambda_k^{*}\sigma_k^2}{\rho_k} + \frac{\nu_k^{*}e_k}{\eta_k(1-\rho_k)}. \tag{B.7}$$

From now, the proof steps are similar to Appendix C of [11]. We briefly introduce the important logic and properties that are used to prove Proposition 1. By observing problem (B.7), we can show that two cases of optimal Lagrange multipliers, $(\lambda_k^{*} = 0, \nu_k^{*} > 0)$ and $(\lambda_k^{*} > 0, \nu_k^{*} = 0)$ cannot happen for any k. And the optimal value of problem (B.6) should be a nontrivial lower bound on the primal optimal value, so that we need $\boldsymbol{A}_k^{*} \succeq 0$ and $\mathrm{Tr}(\boldsymbol{A}_k^{*}\boldsymbol{X}_k^{*}) = 0$, then

$$\boldsymbol{A}_k^{*}\boldsymbol{X}_k^{*} = 0, \forall k. \tag{B.8}$$

Let us assume that $\lambda_k^{*} = \nu_k^{*} = 0, \forall k$. From (B.5), $\boldsymbol{A}_k^{*} = \boldsymbol{V}_{\mathrm{RF}}^{H}\boldsymbol{V}_{\mathrm{RF}}$. Since we assumed $\mathrm{rank}(\boldsymbol{V}_{\mathrm{RF}}) = N_{\mathrm{RF}}$, $\mathrm{rank}(\boldsymbol{A}_k^{*}) = N_{\mathrm{RF}}$, then from (B.8), $\boldsymbol{X}_k^{*} = 0$ which should not be the optimal to problem (17). Therefore, at least one k exists such that $\lambda_k^{*} > 0$ and $\nu_k^{*} > 0$. Now, we define

$$\boldsymbol{B}^{*} = \boldsymbol{V}_{\mathrm{RF}}^{H}\boldsymbol{V}_{\mathrm{RF}} + \sum_{l=1}^{k}(\lambda_l - \nu_l)\boldsymbol{V}_{\mathrm{RF}}^{H}\boldsymbol{h}_l\boldsymbol{h}_l^{H}\boldsymbol{V}_{\mathrm{RF}}, \tag{B.9}$$

then,

$$\boldsymbol{A}_k^{*} = \boldsymbol{B}^{*} - \left(\frac{\lambda_k^{*}}{\gamma_k} + \lambda_k^{*}\right)\boldsymbol{V}_{\mathrm{RF}}^{H}\boldsymbol{h}_k\boldsymbol{h}_k^{H}\boldsymbol{V}_{\mathrm{RF}}. \tag{B.10}$$

Since $\boldsymbol{A}_k^{*} \succeq 0$ and $\left(\frac{\lambda_k^{*}}{\gamma_k} + \lambda_k^{*}\right)\boldsymbol{V}_{\mathrm{RF}}^{H}\boldsymbol{h}_k\boldsymbol{h}_k^{H}\boldsymbol{V}_{\mathrm{RF}} \succeq 0$, it is true that $\boldsymbol{B}^{*} \succeq 0$.

Let us suppose $\exists \boldsymbol{x} \neq 0$ such that $\boldsymbol{x}^{H}\boldsymbol{B}^{*}\boldsymbol{x} = 0$. Since $\boldsymbol{x}^{H}\boldsymbol{A}_k^{*}\boldsymbol{x} \geq 0$, $\boldsymbol{x}^{H}\boldsymbol{V}_{\mathrm{RF}}^{H}\boldsymbol{h}_k\boldsymbol{h}_k^{H}\boldsymbol{V}_{\mathrm{RF}}\boldsymbol{x} = 0$ for k s.t. $\lambda_k^{*} > 0$.

On the other hand, using (B.9), $\boldsymbol{x}^H\boldsymbol{B}^*\boldsymbol{x} = \boldsymbol{x}^H\boldsymbol{V}_{\mathrm{RF}}^H\boldsymbol{V}_{\mathrm{RF}}\boldsymbol{x} = ||\boldsymbol{V}_{\mathrm{RF}}\boldsymbol{x}||^2 \geq 0$. Since rank $(\boldsymbol{V}_{\mathrm{RF}}) = N_{\mathrm{RF}}$, $\boldsymbol{V}_{\mathrm{RF}}\boldsymbol{x} \neq 0$ for $\boldsymbol{x} \neq 0$, then $\boldsymbol{x}^H\boldsymbol{B}^*\boldsymbol{x} > 0$. This contradicts with our assumption, $\boldsymbol{x}^H\boldsymbol{B}^*\boldsymbol{x} = 0$. Therefore, $\boldsymbol{B}^* \succ 0$, that is, $\boldsymbol{B}^*$ is a full-rank matrix.

For k s.t. $\lambda_k^* = \nu_k^* = 0$, $\mathrm{rank}(\boldsymbol{A}_k^*) = \mathrm{rank}(\boldsymbol{B}^*) = N_{\mathrm{RF}}$. From (B.8), we obtain $\boldsymbol{X}_k^* = 0$, however, this cannot be the optimal primal solution. So, for any k, the case of $\lambda_k^* = \nu_k^* = 0$ does not happen. Therefore, it is true that $\lambda_k^* > 0$ and $\nu_k^* > 0$, $\forall k$. Due to complementary slackness, the primal optimal solutions satisfy equality for the SINR constraints and harvest energy constraints in problem (17). This proves the first part of Proposition 1.

From (B.10), $N_{\mathrm{RF}} \geq \mathrm{rank}(\boldsymbol{A}_k^*) \geq N_{\mathrm{RF}} - 1$. If $\mathrm{rank}(\boldsymbol{A}_k^*) = N_{\mathrm{RF}}$, $\boldsymbol{X}_k^* = \boldsymbol{0}$ which does not make sense. Hence, $\mathrm{rank}(\boldsymbol{A}_k^*) = N_{\mathrm{RF}} - 1$ and $\mathrm{rank}(\boldsymbol{X}_k^*) = 1$ from (B.8). This proves the second part of Proposition 1.

APPENDIX C
C. SOLVING PROBLEM (23)

Let us denote $\boldsymbol{A} = \boldsymbol{V}_{\mathrm{RF}}\tilde{\boldsymbol{V}}_{\mathrm{Dig}}$. Diagonal elements of $\boldsymbol{A}^H\boldsymbol{A}$ are positive or zero. Then, the objective function, $\mathrm{Tr}(\boldsymbol{A}^H\boldsymbol{A}\boldsymbol{P})$ becomes $\sum_k \alpha_k p_k$ where α_k is the kth diagonal element of $\boldsymbol{A}^H\boldsymbol{A}$. Since p_k is not coupled with p_l $\forall l \neq k$ in the objective function and the constraints in problem (23) are decoupled over k as well, we can decompose problem (23) into K subproblems. So, a subproblem for a given k is formulated as

$$\min_{\{p_k,\rho_k\}} \quad p_k \tag{C.1a}$$

$$\text{s. t.} \quad p_k \geq \gamma_k\left(\sigma_k^2 + \frac{\delta_k^2}{\rho_k}\right), \tag{C.1b}$$

$$p_k \geq \frac{e_k}{\eta_k(1-\rho_k)} - \sigma_k^2, \tag{C.1c}$$

$$0 \leq \rho_k \leq 1. \tag{C.1d}$$

The optimal solution for problem (23) makes constraints (C.1b) and (C.1c) active. Then, the following equation is obtained

$$\gamma_k\left(\sigma_k^2 + \frac{\delta_k^2}{\rho_k}\right) = \frac{e_k}{\eta_k(1-\rho_k)} - \sigma_k^2 \tag{C.2}$$

which is a quadratic equation of ρ_k. For $0 \leq \rho_k \leq 1$, the solution of (C.2) was found in Appendix D of [11].

REFERENCES

[1] R. J. Vyas, B. B. Cook, Y. Kawahara, and M. M. Tentzeris, "E-WEHP: A batteryless embedded sensor-platform wirelessly powered from ambient digital-TV signals," *IEEE Trans. Microw. Theory Techn.*, vol. 61, no. 6, pp. 2491–2505, Jun. 2013.

[2] C. R. Valenta and G. D. Durgin, "Harvesting wireless power: Survey of energy-harvester conversion efficiency in far-field, wireless power transfer systems," *IEEE Microw. Mag.*, vol. 15, no. 4, pp. 108–120, Jun. 2014.

[3] *Future Technology Trends of Terrestrial International Mobile Telecommunications Systems Towards 2030 and Beyond*, ITU-R WP5D, International Telecommunication Union, Report document M.2516-0, Nov. 2022.

[4] *Study on Ambient Power-Enabled Internet of Things*, document TR 22.840, 3GPP, Release 19, Jun. 2023.

[5] M. Z. Chowdhury, M. Shahjalal, S. Ahmed, and Y. M. Jang, "6G wireless communication systems: Applications, requirements, technologies, challenges, and research directions," *IEEE Open J. Commun. Soc.*, vol. 1, pp. 957–975, 2020.

[6] C. Yeh, G. D. Jo, Y.-J. Ko, and H. K. Chung, "Perspectives on 6G wireless communications," *ICT Exp.*, vol. 9, no. 1, pp. 82–91, Feb. 2023.

[7] J. Hu, Q. Wang, and K. Yang, "Energy self-sustainability in full-spectrum 6G," *IEEE Wireless Commun.*, vol. 28, no. 1, pp. 104–111, Feb. 2021.

[8] S. Özyurt, A. F. Coskun, S. Büyüçorak, G. K. Kurt, and O. Kucur, "A survey on multiuser SWIPT communications for 5G+," *IEEE Access*, vol. 10, pp. 109814–109849, 2022.

[9] Y. Zheng, S. A. Tegos, Y. Xiao, P. D. Diamantoulakis, Z. Ma, and G. K. Karagiannidis, "Zero-energy device networks with wireless-powered RISs," *IEEE Trans. Veh. Technol.*, vol. 72, no. 10, pp. 13655–13660, Oct. 2023.

[10] R. Zhang and C. K. Ho, "MIMO broadcasting for simultaneous wireless information and power transfer," *IEEE Trans. Wireless Commun.*, vol. 12, no. 5, pp. 1989–2001, May 2013.

[11] Q. Shi, L. Liu, W. Xu, and R. Zhang, "Joint transmit beamforming and receive power splitting for MISO SWIPT systems," *IEEE Trans. Wireless Commun.*, vol. 13, no. 6, pp. 3269–3280, Jun. 2014.

[12] Z. Zong, H. Feng, F. R. Yu, N. Zhao, T. Yang, and B. Hu, "Optimal transceiver design for SWIPT in K-user MIMO interference channels," *IEEE Trans. Wireless Commun.*, vol. 15, no. 1, pp. 430–445, Jan. 2016.

[13] K. Humadi, I. Trigui, W.-P. Zhu, and W. Ajib, "Simultaneous wireless information and power transfer in mmWave networks under user-centric base station clustering," *IEEE Trans. Wireless Commun.*, vol. 22, no. 3, pp. 1823–1840, Mar. 2023.

[14] J. Liu, K. Xiong, Y. Lu, D. W. K. Ng, Z. Zhong, and Z. Han, "Energy efficiency in secure IRS-aided SWIPT," *IEEE Wireless Commun. Lett.*, vol. 9, no. 11, pp. 1884–1888, Nov. 2020.

[15] J. Tang, J. Luo, M. Liu, D. K. C. So, E. Alsusa, G. Chen, K.-K. Wong, and J. A. Chambers, "Energy efficiency optimization for NOMA with SWIPT," *IEEE J. Sel. Topics Signal Process.*, vol. 13, no. 3, pp. 452–466, Jun. 2019.

[16] Y. Guo, C. Skouroumounis, and I. Krikidis, "A coverage area-based CoMP technique for SWIPT-enabled mobile networks," *IEEE Trans. Green Commun. Netw.*, vol. 7, no. 4, pp. 2473–2400, Dec. 2023.

[17] D. Gesbert, M. Kountouris, R. W. Heath, C.-B. Chae, and T. Salzer, "Shifting the MIMO paradigm," *IEEE Signal Process. Mag.*, vol. 24, no. 5, pp. 36–46, Sep. 2007.

[18] T. L. Marzetta, "Noncooperative cellular wireless with unlimited numbers of base station antennas," *IEEE Trans. Wireless Commun.*, vol. 9, no. 11, pp. 3590–3600, Nov. 2010.

[19] J. Wang, Z. Lan, C.-W. Pyo, T. Baykas, C.-S. Sum, M. A. Rahman, J. Gao, R. Funada, F. Kojima, H. Harada, and S. Kato, "Beam codebook based beamforming protocol for multi-Gbps millimeter-wave WPAN systems," *IEEE J. Sel. Areas Commun.*, vol. 27, no. 8, pp. 1390–1399, Oct. 2009.

[20] S. Hur, T. Kim, D. J. Love, J. V. Krogmeier, T. A. Thomas, and A. Ghosh, "Millimeter wave beamforming for wireless backhaul and access in small cell networks," *IEEE Trans. Commun.*, vol. 61, no. 10, pp. 4391–4403, Oct. 2013.

[21] O. E. Ayach, S. Rajagopal, S. Abu-Surra, Z. Pi, and R. W. Heath, "Spatially sparse precoding in millimeter wave MIMO systems," *IEEE Trans. Wireless Commun.*, vol. 13, no. 3, pp. 1499–1513, Mar. 2014.

[22] F. Sohrabi and W. Yu, "Hybrid digital and analog beamforming design for large-scale antenna arrays," *IEEE J. Sel. Topics Signal Process.*, vol. 10, no. 3, pp. 501–513, Apr. 2016.

[23] X. Wu, D. Liu, and F. Yin, "Hybrid beamforming for multi-user massive MIMO systems," *IEEE Trans. Commun.*, vol. 66, no. 9, pp. 3879–3891, Sep. 2018.

[24] A. A. Nasir, H. D. Tuan, T. Q. Duong, H. V. Poor, and L. Hanzo, "Hybrid beamforming for multi-user millimeter-wave networks," *IEEE Trans. Veh. Technol.*, vol. 69, no. 3, pp. 2943–2956, Mar. 2020.

[25] B.-Y. Chen, Y.-F. Chen, and S.-M. Tseng, "Hybrid beamforming and data stream allocation algorithms for power minimization in multi-user massive MIMO-OFDM systems," *IEEE Access*, vol. 10, pp. 101898–101912, 2022.
[26] P. Zhang, L. Pan, T. Laohapensaeng, and M. Chongcheawchamnan, "Hybrid beamforming based on an unsupervised deep learning network for downlink channels with imperfect CSI," *IEEE Wireless Commun. Lett.*, vol. 11, no. 7, pp. 1543–1547, Jul. 2022.
[27] R. Li, B. Guo, M. Tao, Y.-F. Liu, and W. Yu, "Joint design of hybrid beamforming and reflection coefficients in RIS-aided mmWave MIMO systems," *IEEE Trans. Commun.*, vol. 70, no. 4, pp. 2404–2416, Apr. 2022.
[28] A. Li and C. Masouros, "Energy-efficient SWIPT: From fully digital to hybrid analog–digital beamforming," *IEEE Trans. Veh. Technol.*, vol. 67, no. 4, pp. 3390–3405, Apr. 2018.
[29] Ö. T. Demir and T. E. Tuncer, "Antenna selection and hybrid beamforming for simultaneous wireless information and power transfer in multi-group multicasting systems," *IEEE Trans. Wireless Commun.*, vol. 15, no. 10, pp. 6948–6962, Oct. 2016.
[30] G. Kwon, H. Park, and M. Z. Win, "Joint beamforming and power splitting for wideband millimeter wave SWIPT systems," *IEEE J. Sel. Topics Signal Process.*, vol. 15, no. 5, pp. 1211–1227, Aug. 2021.
[31] Z. Chen, J. Tang, N. Zhao, M. Liu, and D. K. C. So, "Hybrid beamforming with discrete phase shifts for RIS-assisted multiuser SWIPT system," *IEEE Wireless Commun. Lett.*, vol. 12, no. 1, pp. 104–108, Jan. 2023.
[32] M. Grant, S. Boyd, and Y. Ye. (2015). *CVX: MATLAB Software for Disciplined Convex Programming (2008)*. [Online]. Available: http://stanford.edu/boyd/cvx
[33] L. Liang, W. Xu, and X. Dong, "Low-complexity hybrid precoding in massive multiuser MIMO systems," *IEEE Wireless Commun. Lett.*, vol. 3, no. 6, pp. 653–656, Dec. 2014.
[34] B. Aharon and A. Nemirovski, *Lectures on Modern Convex Optimization*. PA, USA: Siam, 2001.
[35] X. Li, S. Wang, and Y. Cai, "Tutorial: Complexity analysis of singular value decomposition and its variants," 2019, *arXiv:1906.12085*.

SEONG HWAN KIM (Member, IEEE) received the B.S. degree in electrical engineering from Korea University, in 2006, and the M.S. and Ph.D. degrees in electrical engineering and computer science from KAIST, in 2008 and 2013, respectively. From 2016 to 2020, he was an Assistant Professor with the Department of Information and Communication Engineering, Gyeongsang National University, South Korea. Since 2020, he has been an Associate Professor with the Major of Data Science, Korea National University of Transportation. His research interests include vehicular communications, the Internet of Things, and artificial intelligence.

HU JIN (Senior Member, IEEE) received the B.E. degree in electronic engineering and information science from the University of Science and Technology of China, Hefei, China, in 2004, and the M.S. and Ph.D. degrees in electrical engineering from the Korea Advanced Institute of Science and Technology, Daejeon, South Korea, in 2006 and 2011, respectively. From 2011 to 2013, he was a Postdoctoral Fellow with The University of British Columbia, Vancouver, BC, Canada. From 2013 to 2014, he was a Research Professor with Gyeongsang National University, Tongyeong, South Korea. Since 2014, he has been with the School of Electrical Engineering, Hanyang University ERICA, Ansan, South Korea, where he is currently a Professor. His research interests include medium-access control and radio resource management for random access networks and scheduling systems considering advanced signal processing and queueing performance.